Liu *et al. Microstructures* **2025**, *5*, 2025061
DOI: 10.20517/microstructures.2024.142

Microstructures

Review

Open Access

Check for updates

Emerging perovskite color converter for next-generation wireless communications

Ruifeng Liu[1,#], Zijun Yan[1,#], Tingwei Lu[1], Guolong Chen[1], Jianghui Zheng[1], Shuli Wang[1], Yue Lin[1,3], Yuhan Su[1], Xinqin Liao[1], Yijun Lu[1], Hao-Chung Kuo[2], Zhong Chen[1,3], Tingzhu Wu[1,3]

[1]Department of Electronic Science, School of Electronic Science and Technology, Xiamen University, Xiamen 361005, Fujian, China.
[2]Department of Photonics and Graduate Institute of Electro-Optical Engineering, College of Electrical and Computer Engineering, National Yang Ming Chiao Tung University, Hsinchu 30010, Taiwan.
[3]Innovation Laboratory for Sciences and Technologies of Energy Materials of Fujian Province (IKKEM), Xiamen 361005, Fujian, China.
[#]These authors contributed equally to this work.

Correspondence to: Prof. Tingzhu Wu, Department of Electronic Science, School of Electronic Science and Technology, Xiamen University, No. 422 Siming South Road, Xiamen 361005, Fujian, China; Innovation Laboratory for Sciences and Technologies of Energy Materials of Fujian Province (IKKEM), No. 4221, Xiang'an South Road, Xiamen 361005, Fujian, China. E-mail: wutingzhu@xmu.edu.cn

How to cite this article: Liu, R.; Yan, Z.; Lu, T.; Chen, G.; Zheng, J.; Wang, S.; Lin, Y.; Su, Y.; Liao, X.; Lu, Y.; Kuo, H. C.; Chen, Z.; Wu, T. Emerging perovskite color converter for next-generation wireless communications. *Microstructures* **2025**, *5*, 2025061. https://dx.doi.org/10.20517/microstructures.2024.142

Received: 30 Nov 2024 **First Decision:** 25 Mar 2025 **Revised:** 10 Apr 2025 **Accepted:** 23 Apr 2025 **Published:** 7 May 2025

Academic Editor: Zhihua Sun **Copy Editor:** Shu-Yuan Duan **Production Editor:** Shu-Yuan Duan

Abstract

Color converters are indispensable components in photoluminescence white-light devices. As optical wireless communication (OWC) systems leveraging solid-state lighting (SSL) continue to evolve, the development of next-generation color conversion materials has become a pressing priority to meet the stringent requirements for both high-quality illumination and high-speed data transmission. Halide perovskite quantum dots (PQDs) have emerged as promising candidates due to their exceptional color purity, high photoluminescence quantum yield, and fast response time. However, the commercial viability of PQD-based SSL-OWC systems is persistently impeded by several challenges, such as insufficient modulation bandwidth, inadequate long-term stability, and reliance on toxic elements. This review delves into the applications of PQD-based color converters within the realm of OWC. Initially, we conduct a theoretical investigation into the factors that influence the modulation bandwidth and transmission rate of PQD-based systems, revealing the significance of reducing PQD particle sizes in enhancing these parameters. Subsequently, we provide a comprehensive overview of optimization strategies across four critical aspects: the selection of excitation sources, the refinement of PQD structure and encapsulation, the

deployment of modulation schemes and multiplexing techniques, and the advancement of lead-free PQD alternatives. Finally, we summarize different types of PQD-based OWC applications, including white-light-based visible light communication transmitters, underwater wireless optical communication transmitters, and color-converting photodetectors. These applications underscore the dual functionality of PQD layers in both illumination and the facilitation of wavelength-tunable OWC.

Keywords: Perovskite quantum dots, optical wireless communication, color converter, visible light communication, white-light system, solid-state lighting

INTRODUCTION

In recent years, the burgeoning field of 6G network technology has set its sights on achieving not only ultra-high-speed data transmission but also comprehensive multi-dimensional spatial coverage, spanning from indoor environments to terrestrial, underwater, and even extraterrestrial domains[1,2]. Compared to traditional radio-frequency (RF) communication methods, optical wireless communication (OWC) boasts a significantly larger available spectrum and offers multiple advantages, such as high area capacity, resistance to electromagnetic interference, enhanced physical security, and rapid deployment capability. These attributes render OWC systems a compelling contender for the hardware infrastructure of 6G networks[1,3-5]. Semiconductor light sources, such as light-emitting diodes (LEDs) - including micro light-emitting diodes (μLEDs) - and laser diodes (LDs), serve as ideal OWC transmitter sources, featuring rapid response time, high-speed transmission capabilities, ease of integration, and multifunctional application potential[6-8].

Semiconductor lighting has become an integral part of daily life. Solid-state lighting (SSL) based on LEDs has been established as the dominant technology, attributed to its superior brightness, high efficiency, compact size, extended lifespan, and cost-effectiveness[9,10]. Therefore, the existing SSL infrastructure can be effectively implemented for indoor visible light communication (VLC) systems[2,10]. Embedded VLC systems transmit signals through imperceptible rapid brightness variations superimposed on constant illumination output, causing virtually no impact on the original lighting quality. SSL devices emit white light through the combination of various wavelengths, with one method being the monolithic integration of red, green, and blue (RGB) chips to generate electroluminescence (EL) white light[11]. However, extensive studies have identified multiple technical challenges in white light-emitting diodes (WLEDs) utilizing this approach, including efficiency droop, the "green gap" phenomenon, process compatibility issues, driver circuit design complexity, and aging-induced color shift[12-16]. Alternatively, photoluminescence (PL) WLEDs utilizing color converters have demonstrated enhanced immunity to the aforementioned limitations, thereby solidifying their position as the preferred option in commercial WLED applications[9].

PL WLEDs are implemented through the fluorescent color conversion layer technique, which employs a single blue or ultraviolet (UV) light source to photoexcite fluorescent materials. These materials exhibit radiative emission at longer wavelengths, generating a combined spectral output that results in white light[15,17]. Phosphors are the prevalent color conversion materials in use; however, their deep trap energy states cause a delayed radiative relaxation, leading to afterglow that persists for several microseconds and restricts their operational bandwidth to a few MHz[9,18]. To meet the demands for high-quality white-light illumination and high-speed VLC, there is a pressing need to explore novel categories of color conversion materials with the following requirements: (i) a broad absorption spectrum efficiently utilizing blue or UV excitation sources; (ii) a high photoluminescence quantum yield (PLQY) to achieve superior energy efficiency, high brightness, and low signal-to-noise ratio (SNR); (iii) a wide emission spectrum to satisfy color rendering needs; (iv) fast response characteristics to facilitate high-speed data transmission[19].

Halide perovskite quantum dots (PQDs), with the typical chemical formula ABX_3 (where A is a monovalent cation or organic group, B is a divalent cation, and X is a halide ion such as Cl^-, Br^-, or I^-), have garnered significant attention in the field of optoelectronics attributed to their broad absorption spectra, high PLQY, and nanosecond fluorescence lifetimes compared with II-VI semiconductor QDs and organic emitters[20-22]. PQDs exhibit narrow full width at half maximum (FWHM), typically less than 30 nm, enabling them to display highly saturated colors, with their RGB emissions forming a triangle on the Commission Internationale de l'Eclairage (CIE) chromaticity diagram that spans 140% of the National Television Standards Committee (NTSC) color gamut[23]. For white-light illumination, the spectral distribution can be expanded by combining PQDs with different emission wavelengths, enabling exhaustive coverage of the gaps between peak wavelengths[24,25]. Furthermore, the emission wavelengths of PQDs can be precisely tuned by adjusting the halide elemental ratio. With Br-only perovskites serving as the reference, increasing the Cl content results in a blue shift, while increasing the I content leads to a red shift[25-28]. This tunability enables PQDs to control the spectral distribution accurately, thereby achieving specific correlated color temperature (CCT) for warm or cold white light[25,26].

In addition to exceptional optical properties, the nanosecond PL lifetimes of PQDs enable high modulation bandwidths of nearly 1 GHz. PQD-based white-light systems with data transmission rates exceeding Gbps have been demonstrated for VLC applications[29-32] since Dursun *et al.* first combined perovskite nanocrystals (PNCs) with a LD to achieve a 2 Gbps system in 2016[29]. Following their emergence at the hybrid applications of SSL-VLC, PQD-based color converters have been progressively deployed across other OWC modalities, including underwater wireless optical communication (UWOC)[33,34] and ultraviolet light communication[35,36]. These OWC systems are commonly integrated with emerging devices for monochromatic illumination[37,38], white-light illumination[39-42], or full-color displays[43], with PQDs serving as key color-converting components. Moreover, PQDs provide feasibility for OWC systems to switch wavelengths to maintain optimal communication performance[33-35,44]. A comprehensive overview of representative PQD-based OWC applications is presented in Table 1.

While PQDs have shown promise for high-quality illumination and high-speed data transmission in OWC applications, their instability has limited their broader adoption. Upon exposure to external environmental factors, including oxygen, water, heat, and light irradiation, perovskite materials exhibit susceptibility to decomposition, aggregation, and ion migration, culminating in fluorescence quenching[21,49]. In contrast to organic-inorganic hybrid perovskites, all-inorganic perovskites possess higher binding energies and defect tolerance, resulting in significantly improved stability[21]. However, their long-term stability under complex operating conditions remains insufficient for practical applications[33]. Additionally, prevalent perovskite materials like $CsPbX_3$ contain toxic elements such as lead and cesium, which pose pollution risks throughout the product lifecycle[20,42,45]. To commercialize PQD-based SSL-OWC systems, stability and environmental friendliness are also crucial focuses, alongside enhanced illumination performance and data transmission rates.

In this review, we comprehensively examine the applications of PQD-based color converters in OWC, as schematically depicted in Figure 1. Primarily, we theoretically analyze the factors affecting the modulation bandwidth and data transmission rate of PQD-based systems, identifying potential avenues for enhancement. Reducing the PQD particle sizes to enhance the quantum confinement effect can accelerate the response of the PQD layer, thereby improving the overall modulation bandwidth of the mixed-light system. Additionally, the use of appropriate modulation schemes and multiplexing techniques can fully utilize the channel capacity to improve the data transmission rates. Furthermore, we introduce the design considerations for components of PQD-based transmitters, including the selection of excitation light

Table 1. Summary of typical PQDs applications as color converters for OWC systems

Year	Application type	Emitting materials/Wavelength (nm)	Light source/Wavelength (nm)	Bandwidth	Data rate	Refs.
2018	WLED-VLC	$CsPbBr_{1.8}I_{1.2}$/ ~ 560	μLED/ ~ 445	73 MHz	300 Mbps	[39]
2019	VLC	$CsPbBr_3$-in-Cs_4PbBr_6/520	LD/450	41 MHz	560 Mbps	[37]
2019	UV OWC	$CsPbBr_3$/506	UV/278	70.92 MHz	34 Mbps	[35]
2021	UWOC	$CsPbBr_3$-glass/ ~ 514	LD/450	180 MHz	185 Mbps	[33]
2021	WLED-VLC	DDAB-$CsPbBr_3$/SiO_2/ ~ 515	LED/ ~ 450	1.5 MHz	5.9 Mbps	[40]
2021	FCD-VLC	$CsPbBr_3$-SiO_2/520 $CsPbBrI_2$-SiO_2/660	μLED/ ~ 450	-	1.2 Gbps	[43]
2021	WLED-VLC	$CsPb(Br/I)_3$-PMMA/560 $CsPbI_3$-PMMA/672	μLED/ ~ 470	347 MHz 822 MHz	1.7 Gbps	[31]
2021	WLED-VLC	$CsPbBr_3$ paper/528	μLED/441	229 MHz	400 Mbps	[41]
2022	UWOC	Liquid $CsPbBr_3$/522	LD/440	6 MHz	60 Mbps	[34]
2022	WLD-VLC	Liquid $CsPbBr_3$/511	LD/451	883 MHz	2.1 Gbps	[32]
2022	WLED-VLC	$Cs_3Cu_2I_5$ SCs/444 $CsCu_2I_3$ SCs/580	UV/300	10.1 MHz	87.7 Mbps	[42]
2023	VLC	$CsPbBr_3$-ethanol/517	LD/450	363.68 MHz	1.25 Gbps	[38]
2023	WLED-VLC	$Cs_3Cu_2Br_5$ SCs/464	UV/300	6.7 MHz	45 Mbps	[45]
2023	UV OWC	$CsPbBr_3$/517	LD/375	42 MHz	100Mbps	[36]
2024	WDM-VLC	Liquid $CsPbBr_3$/515 Liquid $CsPbI_3$/630	LD/450	15.5 MHz 4.5 MHz	100 Mbps	[46]
2024	UWOC	$CsPbBr_3$:F/517	LD/450	-	60 Mbps	[47]
2024	WLED-VLC UWOC	$MAPbBr_3$@PbBr(OH)/529	LD/405	25 MHz	50 Mbps	[48]

UV OWC: ultraviolet-light optical wireless communication; FCD: full-color display device; WLD: white laser diode; WDM: wavelength division multiplexing; DDAB: didodecyldimethylammonium bromide; PMMA: polymethyl methacrylate; SC: single crystal; UV: ultraviolet light emitting diode; LED: light-emitting diode; μLED: micro light-emitting diode; PQD: perovskite quantum dot; WLED: white light-emitting diode; LD: laser diode; VLC: visible light communication; UWOC: underwater wireless optical communication.

sources, the structure and encapsulation optimization of PQD layers, and the integration of modulation schemes and multiplexing, all aimed at bolstering the commercial feasibility of lighting and OWC applications. Notably, significant research efforts have been directed toward the development of lead-free perovskite materials to mitigate environmental concerns. Finally, we provide a comprehensive analysis of PQD-based color converters in OWC applications, including indoor VLC transmitters, UWOC transmitters, and color-converting photodetectors (PDs). These applications underscore the multifunctional role of PQD layers in communication, white-light illumination, and wavelength-matching, showcasing their versatility and potential in the field of OWC.

THEORETICAL ANALYSIS OF MODULATION BANDWIDTH AND DATA RATE IN PQD-BASED SYSTEMS

Modulation bandwidth is a critical parameter for evaluating the performance of a communication system. When PQD-based color converters are integrated into OWC systems as cascaded components, the modulation bandwidth of PQD layers directly impacts the overall bandwidth of the OWC systems, similar to light sources, PDs, and channels. From a microstructural perspective, the modulation bandwidth of PQD layers is intimately correlated with carrier dynamics. The measurement of time-resolved photoluminescence (TRPL) curves provides insights into carrier relaxation kinetics, revealing the photoexcitation decay processes in PQDs. Typically, a bi-exponential decay model is used to fit TRPL curves:

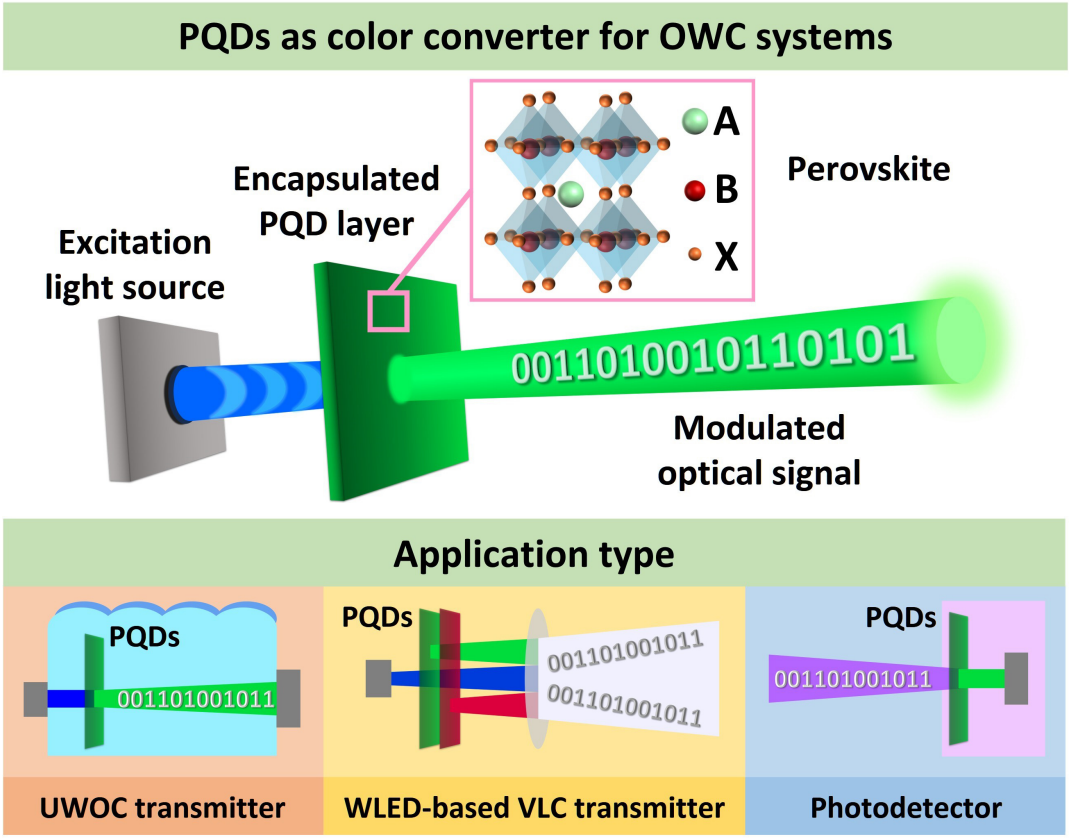

Figure 1. Schematic of the PQD-based color converter implemented in OWC applications. In the lattice structure of perovskite: A is a monovalent cation or organic group such as Cs^+, $CH_3NH_3^+$ (MA^+), or $CH(NH_2)_2^+$ (FA^+), B is a divalent cation such as Pb^{2+}, and X is a halide ion such as Cl^-, Br^-, or I^-. PQD: perovskite quantum dot; OWC: optical wireless communication.

$$I(t) = A_1 \exp\left(-\frac{t}{\tau_1}\right) + A_2 \exp\left(-\frac{t}{\tau_2}\right) \tag{1}$$

where I (t) represents the light intensity as a function of time, τ_1 and τ_2 are the fast and slow decay times, and A_1 and A_2 correspond to the amplitudes of the two decay components. From these parameters, the average PL lifetime (τ) can be calculated:

$$\tau = \frac{A_1\tau_1^2 + A_2\tau_2^2}{A_1\tau_1 + A_2\tau_2} \tag{2}$$

From the perspective of carrier recombination mechanism, τ can be composed of two terms related to radiative and non-radiative recombination[50]:

$$\frac{1}{\tau} = \frac{1}{\tau_{\text{rad}}} + \frac{1}{\tau_{\text{non}}} \tag{3}$$

where τ_{rad} and τ_{non} represent the radiative and non-radiative recombination lifetimes, respectively. A shorter average PL lifetime indicates a faster response time, which is desirable for developing high-bandwidth PQD-based color converters. To reduce τ without compromising PLQY, optimization strategies should focus on shortening τ_{rad} rather than τ_{non}[41]. The nanostructure of PQDs can be optimized to reduce their particle sizes, thereby amplifying the quantum confinement effect and hastening the radiative recombination process[21,51]. On the other side, PQD materials are inherently prone to self-aggregation behavior, leading to a weakened

quantum confinement effect, which causes broadened FWHM, red-shifted emission peak, and prolonged PL lifetime[32,52]. Therefore, promoting uniform distribution of PQDs and suppressing their self-aggregation help maintain fast response characteristics during long-term operation. The frequency response curve of PQDs typically shows low-pass characteristics determined by τ, which can be expressed by the following equation:

$$H(f) = \frac{1}{\sqrt{1 + (2\pi f\tau)^2}} \tag{4}$$

where $H(f)$ represents the response at different frequencies. By setting $H(f) = 1/2$, the theoretical -3 dB bandwidth can be calculated as:

$$f_{-3\ \mathrm{dB}} = \frac{\sqrt{3}}{2\pi\tau} \tag{5}$$

This formula indicates that the theoretical bandwidth is inversely proportional to the average lifetime of the excited states. Under non-ideal conditions, the actual measured bandwidths of PQDs are often lower than the theoretical values due to factors such as the response of the excitation source and resistance-capacitance (RC) in packaged devices. In a complete PQD-based white-light system, the frequency response of the light source and the sensitivity of the PD also influence the bandwidth of the white light, in addition to the color converter. Assuming a single PQD layer, the frequency response of the white light can be expressed as:

$$H_{\mathrm{w}}(f) = H_{\mathrm{source}}(f)\left[\eta + (1-\eta)\frac{S_{\mathrm{conver}}}{S_{\mathrm{source}}}H_{\mathrm{conver}}(f)\right] \tag{6}$$

Where $H_{\mathrm{w}}(f)$, $H_{\mathrm{source}}(f)$ and $H_{\mathrm{conver}}(f)$ represent the frequency responses of the white light, light source, and converter, respectively. η and $1-\eta$ are the optical power components of the light source and converter, while S_{source} and S_{conver} represent the sensitivity indexes of the PD to the two emission wavelengths, assuming the PD has an ideal flat frequency response. As shown in Equation 6, the bandwidth of a mixed-light system cannot exceed that of the light source. While μLEDs or LDs can achieve bandwidths exceeding 1 GHz, PQDs typically exhibit maximum bandwidths at hundreds of MHz[29,31,41,53]. When f surpasses the bandwidth of PQDs, the frequency response of white light experiences significant deterioration. Therefore, improving the bandwidth of PQDs can minimize this deterioration, enabling the modulation bandwidth of white light to approach that of the excitation source.

The transmission data rate is related to the modulation bandwidth and SNR, and is limited by the Shannon-Hartley theorem:

$$C = B \times \log_2(1 + SNR) \tag{7}$$

Where C represents the channel capacity, B is the bandwidth, and SNR is the signal-to-noise ratio. Improving the PLQY of PQDs and the luminance of white light can enhance the SNR. Generally, LDs exhibit a higher SNR than μLEDs, which means that systems employing LDs, with identical bandwidth and modulation schemes, can achieve higher data rates[31,32]. For a specified channel capacity, the implementation of higher-order modulation schemes, such as quadrature amplitude modulation (QAM), can maximize the transmission rate, albeit at the cost of increased hardware and software complexity. Furthermore, the application of multiplexing techniques, including orthogonal frequency division multiplexing (OFDM) and wavelength division multiplexing (WDM), can significantly increase the data rate by multiplying the number of subchannels, despite the added complexity in physical design.

Communication distance and incident angle are also critical parameters to consider. Transmitters with narrow emission angles facilitate higher power density and SNR, which are advantageous for ultra-high-speed directional communication and extending transmission distances. Conversely, transmitters and receivers with broad field-of-view (FoV) angles and omnidirectional capabilities can reduce link alignment requirements, rendering them ideal for multipoint-to-multipoint networking in confined spaces.

PERFORMANCE OPTIMIZATION OF PQD-BASED SSL-OWC SYSTEMS

To enhance the commercial viability of PQD-based SSL-OWC systems, researchers must address several critical areas: improving optical and communication performance, bolstering system reliability, and mitigating potential environmental concerns. The selection of excitation light sources is paramount, as light sources with high bandwidth can maximize the data transmission potential of PQD-based color converters. Various strategies, such as inorganic or organic material coating and liquid-phase fabrication, have been implemented to optimize the structure and encapsulation of PQDs. These approaches aim to reduce PL lifetime, increase modulation bandwidth, enhance stability, and prolong operational lifespan. As the system bandwidth approaches its design limits, advanced modulation schemes and physical multiplexing techniques can be employed to further boost transmission data rates. Additionally, to address environmental concerns, there has been a focus on the development of lead-free perovskite materials, which has shown progress in SSL-OWC applications.

Selection of excitation light sources

The excitation light sources for PQDs can be categorized into two main types: LEDs and LDs. In recent years, μLEDs have emerged as a miniaturized variant of conventional LEDs. LEDs, as mature illumination sources, are characterized by their broad spectral band emission and wide beam divergence, which render them suitable for indoor multi-device communications scenarios[1]. However, the modulation bandwidth of LEDs typically remains constrained to several MHz, as reported in studies[40,54], which is inadequate to meet the 6G communication standards that demand bandwidths exceeding GHz[7,9]. LDs, based on the principle of stimulated emission, are distinguished by their narrow spectrum linewidth, high brightness, strong directionality, and high modulation bandwidth (> GHz), establishing them as viable solutions for high-power, high-quality illumination and long-distance, directional high-speed transmission, such as UWOC[32-34]. Nevertheless, the high cost and intense power density associated with LDs restrict their applicability for indoor lighting applications due to economic and safety considerations.

μLEDs have recently garnered significant attention for their applications in full-color displays, flexible displays, and augmented/virtual reality (AR/VR) applications[14,17]. When integrated into VLC systems, μLEDs achieve higher current densities, substantially reduced RC time constants, and nanosecond carrier lifetimes due to their miniaturized structure, resulting in considerable bandwidth improvements[1,7,8]. By combining μLEDs with specially engineered high-bandwidth PQD layers, μLED-based WLEDs can achieve data transmission rates exceeding Gbps, rivaling the performance of white LDs[31]. Additionally, μLEDs offer ease of integration and scalability, which facilitates the construction of lighting arrays and MIMO communication systems, positioning them as optimal candidates for indoor VLC applications and potential components of Light Fidelity (LiFi) hardware infrastructure[6,7]. However, several challenges, such as the strong quantum-confined Stark effect (QCSE) in GaN-based μLEDs grown on *c*-plane substrates, can compromise the performance of μLEDs[9,15]. The QCSE induces spatial separation of the electron-hole wave function, consequently diminishing radiative recombination rates and decelerating the recombination process. These effects manifest in reduced efficiency and decreased bandwidth. The epitaxial growth of semipolar GaN layers can mitigate the effects of polarization and built-in electric fields, thereby improving the overlap of wave functions and suppressing the occurrence of QCSE[43,55]. Recent investigations have

demonstrated the successful implementation of semipolar μLEDs as light sources in PQD-based VLC systems[41,43,53]. In 2023, Sadhu *et al.* employed a blue semipolar (20-21) μLED with a -3 dB bandwidth of 1.23 GHz as the excitation source[53]. The WLED system, utilizing a color-conversion film composed of $CH_3NH_3PbBr_3$ and two organic emitter materials, achieved a color rendering index (CRI) of 82.4 and a bandwidth of 952 MHz. Beyond semipolar μLEDs, various approaches have been employed to suppress the QCSE, including the implementation of ultra-thin quantum wells[56], nonpolar substrates[57], and nano-engineered InGaN active regions[58]. With advancements in device design and fabrication processes, the modulation bandwidth of μLEDs has recently exceeded 3 GHz[58,59], establishing them as exceptional light sources comparable to LDs.

Optimization of PQD structures

To improve the modulation bandwidth and stability of PQD-based color converters, a variety of strategies have been implemented to refine the structures and encapsulations of PQDs. These include the use of inorganic oxide coating[40,43,51,60], organic polymer encapsulation[30,31,53], inorganic glass embedding[33], nanostructured PQD paper fabrication[41], and solution dispersion[32,34,38,46]. Encapsulating PQDs within a transparent, rigid, and chemically inert inorganic oxide matrix, such as SiO_2, ZrO_2, and Al_2O_3, has proven to be an effective surface passivation method[40,43,51,60]. In 2021, Mo *et al.* synthesized $CsPbBr_3@ZrO_2$ nanocrystals (NCs) at room temperature by injecting $Zr(C_4H_9O)_4$ into $CsPbBr_3$ NCs solution[51]. Figure 2A illustrates the synthesis process of $CsPbBr_3@ZrO_2$ NCs. The PLQY increased from 37% to 80% after ZrO_2 coating. The average size of the NCs decreased from 16.0 nm to 10.1 nm, possibly due to the etching of $CsPbBr_3$ NCs induced by the n-butanol present in $Zr(C_4H_9O)_4$. Numerous studies have demonstrated that reducing the size of QDs intensifies the quantum confinement effect, which leads to decreased PL lifetime[61-64]. Figure 2B shows the TRPL curves of $CsPbBr_3@ZrO_2$ NCs with varying amounts of $Zr(C_4H_9O)_4$. The average PL decay time was decreased from 33.2 ns to as low as 14.2 ns. The stability of $CsPbBr_3@ZrO_2$ NCs was further confirmed, maintaining 81% and 70% of initial PL intensity after 90 min of heating at 60 °C and 70 min of water immersion, respectively.

While the inorganic oxide coating of PQDs significantly improves stability and optical properties, current investigations have not achieved bandwidths exceeding 100 MHz, which suggests that the impact of oxide coating on the bandwidth of PQDs requires further in-depth investigation. To markedly reduce the particle size and PL lifetime of perovskites, thereby increasing modulation bandwidth, the encapsulations of perovskite-polymer composites, particularly using polymethyl methacrylate (PMMA), have gained widespread attention[23,65,66]. PMMA effectively wraps and disperses PQDs via physical interactions, preventing exposure to air while maintaining small particle sizes. In 2021, Wang *et al.* synthesized yellow/red-emitting $CsPb(Br/I)_3$ and $CsPbI_3$ perovskite nanocrystal-polymethyl methacrylate (PNC-PMMA) films[31]. The average particle sizes of $CsPb(Br/I)_3$ and $CsPbI_3$ QDs were 9.30 ± 1.53 and 5.73 ± 0.95 nm, respectively, as shown in Figure 2C and D. Attributed to the accelerated carrier relaxation rates associated with these extremely small particle sizes, the yellow and red PNC-PMMA films achieved PL lifetimes of only 11.2 and 3.5 ns, resulting in high modulation bandwidths of 347 and 822 MHz, respectively. However, upon six-month storage under ambient conditions at room temperature, both PNC-PMMA samples exhibited degradation in frequency response curves and normalized emission spectra, as illustrated in Figure 2E and F. The bandwidths of yellow and red PNC-PMMA films decreased to 230 and 624 MHz, accompanied by a 10 nm blue shift and a 21 nm red shift, respectively. Although PNC-PMMA demonstrated remarkable bandwidth, the inherent high thermal resistance of PMMA can lead to the thermal damage of PNCs, and the self-aggregation of PNCs can increase particle size[33]. These factors contribute to the progressive deterioration of the bandwidth and emission quality of PNC-PMMA films over extended periods.

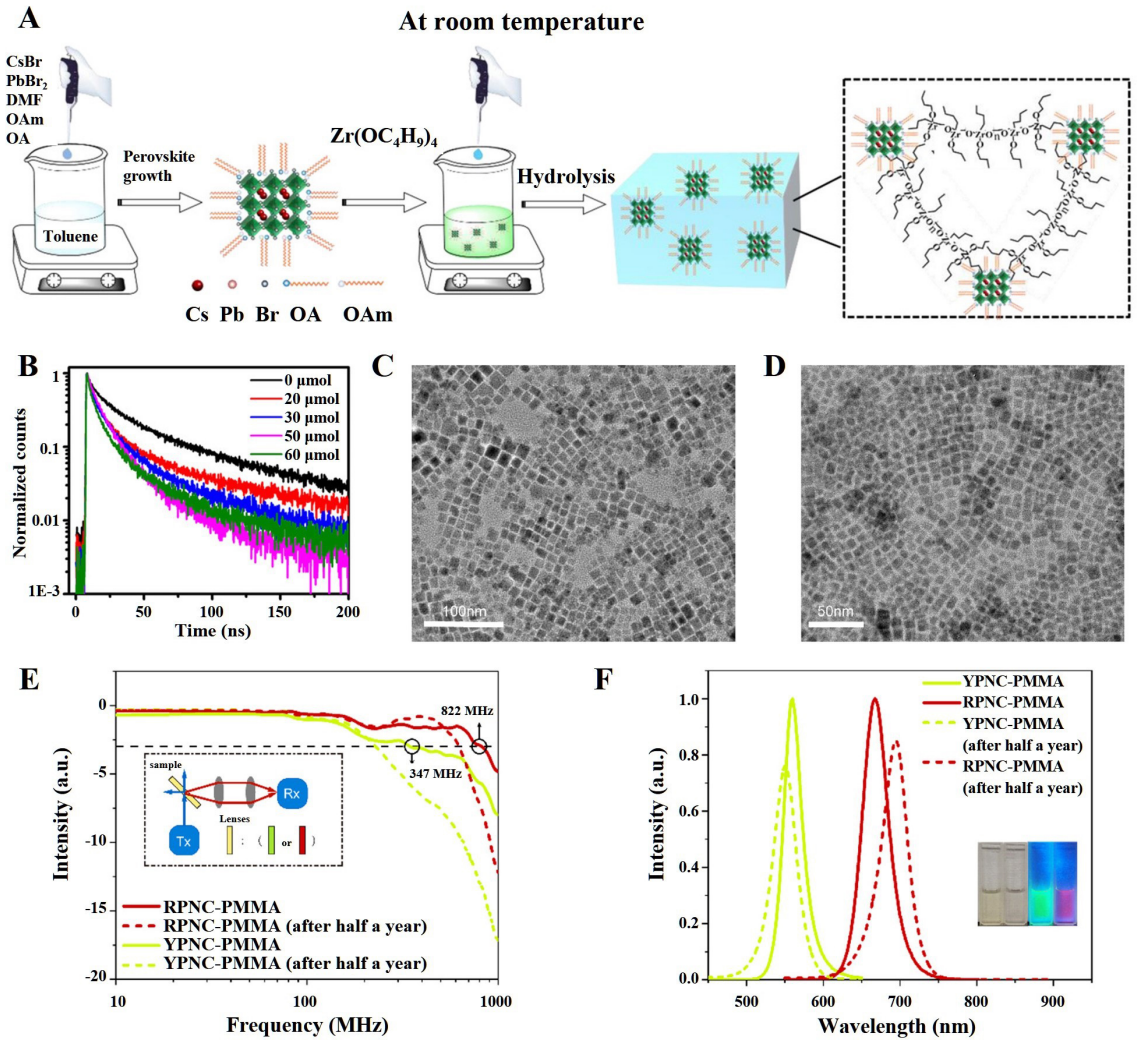

Figure 2. (A) Synthesis process of $CsPbBr_3@ZrO_2$ NCs at room temperature; (B) PL decay curves of $CsPbBr_3@ZrO_2$ NCs with different amounts of $Zr(C_4H_9O)_4$; (C and D) transmission electron microscopy (TEM) images of yellow and red PNCs; (E) frequency response of red and yellow PNC-PMMA, and their bandwidth. Inset is the schematic of the test setup for the bandwidth measurement; (F) emission spectra of red and yellow PNC-PMMA. Insets are the photos of red and yellow PQD samples dispersed in n-hexane under 365-nm UV light irradiation. Reproduced with permission: (A and B)[51], Copyright 2021, Wiley-VCH GmbH; (C-F)[31], Copyright 2021, American Chemical Society. NC: nanocrystal; PQD: perovskite quantum dot; UV: ultraviolet; PNC-PMMA: perovskite nanocrystal-polymethyl methacrylate.

To bolster the long-term stability of PQDs, researchers have developed structures that embed PNCs within the inorganic glass matrix[67-69]. In 2021, Xia *et al.* demonstrated in situ precipitation of $CsPbBr_3$ NCs in inorganic amorphous glass through solid-state reactions[33]. The process schematic and photograph of $CsPbBr_3$ NCs-glass are shown in Figure 3A and B. Embedding $CsPbBr_3$ NCs into an amorphous glass matrix slightly reduces the transmittance of the color converter; however, the water and thermal stability are significantly enhanced. During the water immersion test, the NCs-glass initially experienced appreciable PLQY deterioration (from 68.5% to 56.0% in the first 6 h), attributed to the erosion of NCs that were not completely embedded in the glass. Nevertheless, as the testing period extended from 10 h to 2 weeks, the PLQY of the NCs-glass exhibited minimal change from 53.6% to 53.3%, demonstrating that the glass matrix effectively protected the fully embedded NCs. During another thermal stability test, the NCs-glass was subjected to a temperature increasing from room temperature to 200 °C. Although the luminescence

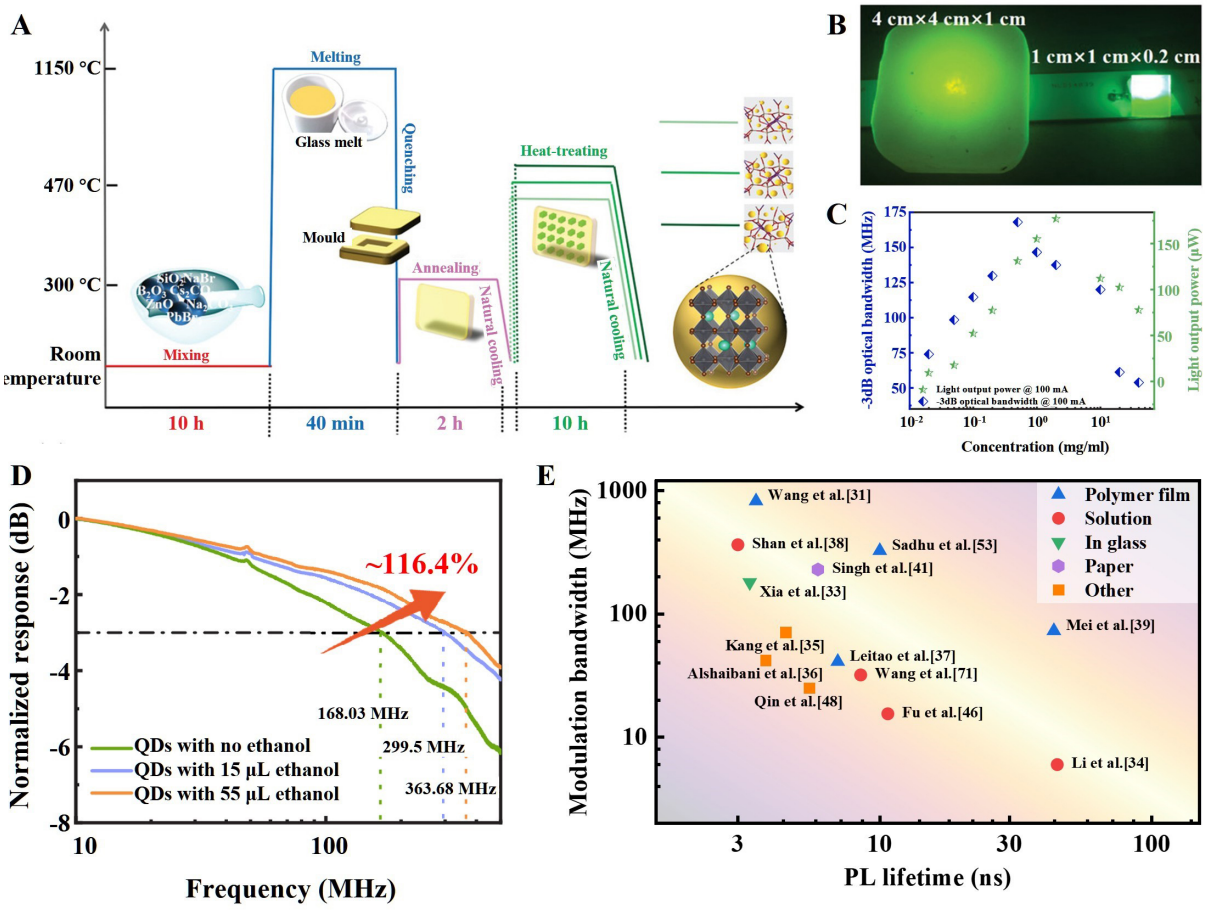

Figure 3. (A) Synthesis process of $CsPbBr_3$ NCs-glass through solid-state reactions; (B) photograph of $CsPbBr_3$ NCs-glass with two sizes; (C) the -3 dB bandwidth and LOP of $CsPbBr_3$ PQDs with different concentrations; (D) frequency response of $CsPbBr_3$ PQDs with different volumes of ethanol; (E) benchmark of the modulation bandwidth versus PL lifetime for PQDs under different encapsulations. Reproduced with permission: (A and B)[33], Copyright 2021, Wiley-VCH GmbH; (C and D)[38], Copyright 2023, Optica Publishing Group. NC: nanocrystal; PQD: perovskite quantum dot; LOP: light output power; PL: photoluminescence.

intensity of NCs decreased with rising temperature, it recovered to its initial value upon cooling to room temperature. Besides its exceptional stability, $CsPbBr_3$ NCs-glass also demonstrated excellent communication performance. The NCs exhibited an average size of only 5.2 nm. Furthermore, the authors emphasized that higher refractive indexes of the matrix can enhance radiative transition rates of $CsPbBr_3$ NCs, thereby reducing their PL decay times. With glass matrix typically having a higher refractive index (1.54) than other matrixes, $CsPbBr_3$ NCs exhibited a minimum decay time of 3.32 ns. Under high-intensity LD excitation, a -3 dB bandwidth of 180 MHz was measured.

In comparison to their solid-phase counterparts, liquid-phase PQDs, which have been extensively investigated in recent years, present several inherent advantages. Firstly, PQDs grown and preserved in solution maintain uniform distribution and suppress self-aggregation, thereby ensuring excellent optical properties and fast response speeds[70]. Secondly, the mobility of PQDs in solution provides convective heat dissipation pathways, demonstrating low thermal resistance and robust heat dissipation capabilities. Liquid PQDs can be encapsulated within dense, rigid cavities such as glass, which further enhances their stability. Moreover, liquid PQDs-glass cavities can be molded into various shapes for color converters, offering flexibility and adaptability[32,38]. Thirdly, liquid PQDs exhibit broad emission angles, enabling wide-angle or

even omnidirectional transmitters that minimize link alignment requirements[34,46,71]. In 2022, Ali *et al.* demonstrated high-bandwidth liquid-phase $CsPbBr_3$ in glass cavities[32]. The bandwidth only marginally decreased from 1020 MHz to 883 MHz when a blue LD was combined with liquid-phase $CsPbBr_3$ color converters. Compared to solid-phase $CsPbBr_3$, liquid-phase $CsPbBr_3$ showed less efficiency droop over time. In 2023, Shan *et al.* investigated the impact of $CsPbBr_3$ PQD concentration in hexane solution on optical performance and modulation bandwidth[38]. As depicted in Figure 3C, both modulation bandwidth and light output power (LOP) increased initially and then decreased with rising PQD concentration, achieving a maximum -3 dB bandwidth of 168.03 MHz at 0.5 mg/mL concentration. Furthermore, when pumped by a 100 mA LD, the addition of ethanol further improved the frequency response and bandwidth of $CsPbBr_3$ PQDs, as illustrated in Figure 3D. After the addition of 55 μL ethanol to 1 ml $CsPbBr_3$ PQDs, possibly attributed to the energy transfer assisted solvent effect, the PQDs achieved a -3 dB bandwidth of 363.68 MHz and a data rate of 1.25 Gbps, despite approximately halved PL intensity. This study reveals the benefits of energy transfer channels for bandwidth improvement, indicating that establishing stable energy transfer pathways in PQD solutions is a promising optimization strategy.

The benchmark of the modulation bandwidth for PQDs under different encapsulations is summarized in Figure 3E. With ongoing advancements in nano-engineering aimed at minimizing PL lifetimes, the modulation bandwidth of perovskite color converters is anticipated to exceed 1 GHz. Meanwhile, the enhancements in optical properties and stability achieved via different encapsulation strategies demand further in-depth investigation[72]. In addition to the widely adopted polymer-film-based and solution-phase PQDs, alternative architectures of perovskite color converters warrant attention. For instance, perovskite-on-polymer microspheres, distinguished by their unique light diffusion properties, demonstrate a uniform light intensity distribution across a broad range of viewing angles, offering promising potential for applications of SSL and liquid-crystal display backlighting[66,73].

Modulation schemes and multiplexing

Researchers have optimized the frequency response of systems through improvements in semiconductor light sources and PQD-based color converters. Furthermore, by selecting appropriate modulation schemes and multiplexing techniques, data transmission rates can be substantially increased, occasionally exceeding ten times the -3 dB bandwidth. Non-return-to-zero on-off keying (NRZ-OOK), a fundamental modulation scheme in wireless communications, employs high and low levels to encode sequences of ones and zeros. This straightforward modulation scheme typically enables the transmission rate to achieve twice the modulation bandwidth when the bit-error-rate (BER) is below the typical forward error correction (FEC) threshold of 3.8×10^{-3}.

In pursuit of higher data rates, advanced modulation schemes and multiplexing techniques have been implemented in PQD-based OWC systems[5]. In OFDM technique, which combines modulation and multiplexing, data streams are transmitted across multiple subcarriers that maintain orthogonality, allowing spectral overlap without interference and enhancing spectral utilization efficiency. Bit loading for each subcarrier can be dynamically adjusted according to channel SNR, enabling the selection of different modulation schemes[74]. Typically, low-frequency subcarriers support higher bit loading and can accommodate advanced modulation schemes, such as higher-order QAM, while high-frequency subcarriers with lower bit loading may utilize simpler modulation schemes like low-order QAM and binary phase shift keying (BPSK)[45]. This adaptive bit loading maximizes channel utilization, achieving data rates in certain cases that exceed ten times the bandwidth[37,51]. Nevertheless, OFDM introduces increased complexity in both hardware and software processing. Additionally, the high peak-to-average power ratio of OFDM makes it susceptible to nonlinear distortion and demands high linearity from amplifiers in transmitters[75].

Another multiplexing technique, WDM, has been successfully implemented in RGB-organic light emitting diode (OLED) devices[76,77], multicolor μLED devices[74,78,79], and CdSe QD-based full-color devices[80]. The applications of PQD-based color converters with different wavelengths in SSL systems have also been widely adopted, highlighting the adaptability of WDM. WDM can be effectively combined with lightweight modulation schemes such as NRZ-OOK. Instead of significantly increasing processing complexity, such systems emphasize optical system architecture. By utilizing multiple sets of independently modulated light sources and separate PDs, multiple optical channels at different wavelengths can be established, thereby multiplying the transmission rates. Additional physical multiplexing, such as time division multiplexing and polarization division multiplexing, holds potential for future research and applications. The selection of appropriate excitation sources and PQD structures, along with suitable modulation schemes and multiplexing, enables the optimal SSL-OWC system designs for specific application scenarios.

Lead-free PQDs

The presence of toxic lead in $APbX_3$-type perovskites presents significant environmental hazards throughout their entire life cycle, from manufacture to end-of-life stages. Although improved manufacturing processes, encapsulation methods, and disposal procedures can mitigate lead leakage[43], these solutions increase costs and do not fundamentally resolve the underlying issue. Therefore, the development of lead-free perovskites for lighting and optical communication represents an attractive alternative[81-83]. In recent years, copper halide perovskites, especially zero-dimensional (0D) $Cs_3Cu_2X_5$ and one-dimensional (1D) $CsCu_2X_3$, have emerged for high-quality SSL applications due to their superior optical properties, such as high PLQY, broad spectrum, and low self-absorption[20,83,84]. These materials include green-emitting $Cs_3Cu_2Cl_5$[60], yellow-emitting $CsCu_2I_3$, blue-emitting $Cs_3Cu_2I_5$[42], $Cs_3Cu_2Br_5$[45], and violet-emitting K_2CuBr_3[85], with their integration into VLC systems being actively explored.

In 2022, Wang *et al.* demonstrated UV-excited $Cs_3Cu_2I_5$ and $CsCu_2I_3$ single crystals (SCs) as blue and yellow color converters for WLED[42]. As shown in Figure 4A, they employed a pressure-assisted cooling method to synthesize large copper halide perovskites SCs, reducing the specific surface area to enhance the stability of the resulting materials. Scanning electron microscopy (SEM) images of $Cs_3Cu_2I_5$ and $CsCu_2I_3$ SCs are shown in Figure 4B and C, which exhibit uniform orientation and smooth surfaces of the large SCs, indicating their potential for superior optical performance. Figure 4D displays the electroluminescence spectra of the constructed WLED under various driving voltages, with the broad spectral coverage enabling the WLED to achieve a CRI of 91. In the VLC application, the system demonstrated a -3 dB bandwidth of 10.1 MHz and achieved a data rate of 87.7 Mbps using OFDM modulation. Figure 4E illustrates the frequency response of the VLC system and the captured 10-MHz eye diagram. In 2023, the research group further developed blue-emitting 0D $Cs_3Cu_2Br_5$ SCs[45]. The resulting white-light system achieved a -3 dB bandwidth of 6.7 MHz and a data rate of 45 Mbps using OFDM modulation. Although copper halide perovskite SCs exhibit broadband emission suitable for high-CRI lighting, their PL lifetimes, ranging from tens of nanoseconds to several microseconds, limit their bandwidths to below 100 MHz. Future research should focus on improving the bandwidth of copper halide perovskites through structure optimization. Additionally, alternative lead-free perovskites incorporating Ag^+, Sb^{3+}, or Bi^{3+} as Pb substitutes have been successively developed for WLEDs[20,66,84]. These diverse lead-free perovskites provide more options for color-conversion materials in PQD-based OWC systems. It is anticipated that more non-toxic perovskites will demonstrate high-speed communication capabilities in future research, becoming qualified alternatives to the current high-bandwidth $CsPbX_3$.

OWC APPLICATIONS OF COLOR-CONVERTING PQDS

A typical OWC system consists of three primary elements: transmitter, channel, and receiver. Color

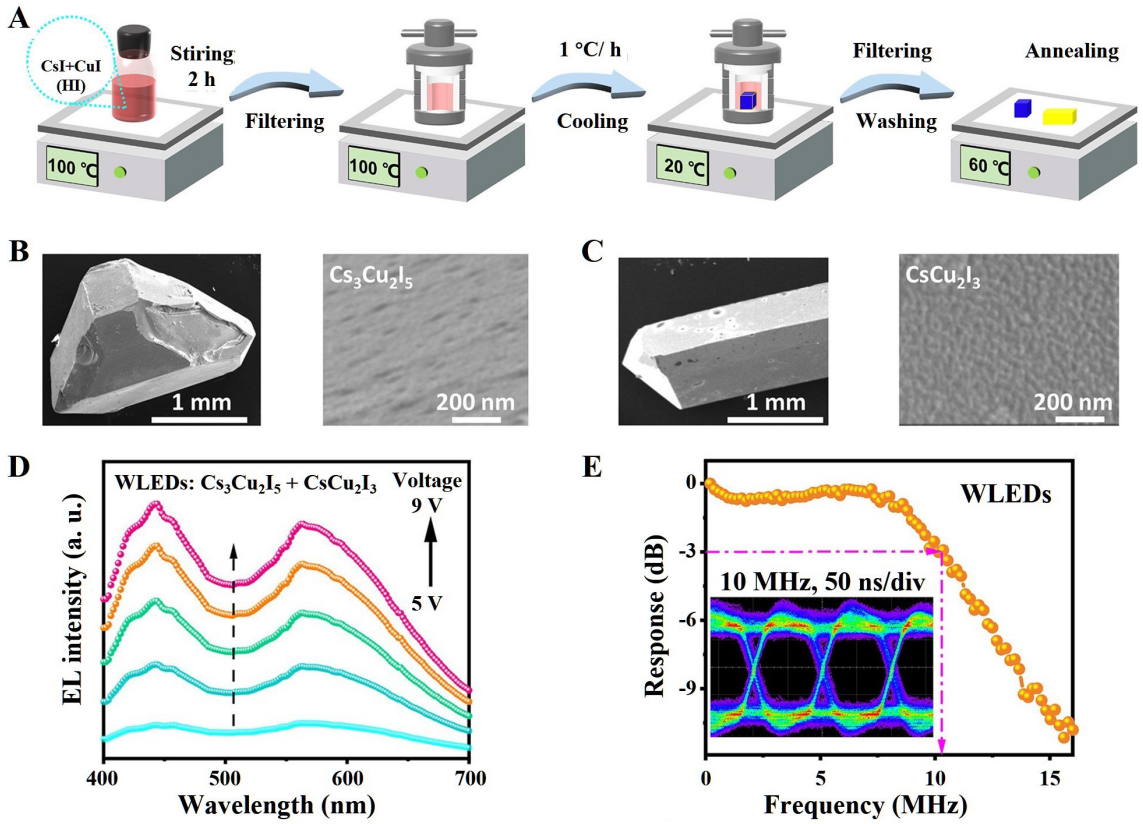

Figure 4. (A) Grown process of $Cs_3Cu_2I_5$ and $CsCu_2I_3$ SCs with pressure-assisted cooling method; (B and C) SEM images of $Cs_3Cu_2I_5$ and $CsCu_2I_3$ SCs grown with pressure-assisted; (D) EL spectra of the WLEDs under various driving voltages; (E) frequency response of the WLEDs. Inset is the captured eye diagram. Reproduced with permission: under a Creative Commons Attribution License[42]. SEM: scanning electron microscopy; SC: single crystal; EL: electroluminescence; WLED: white light-emitting diode.

converters are predominantly integrated into transmitters, where they convert light from excitation sources (including LEDs, LDs and μLEDs) into longer wavelengths. The converted light is subsequently transmitted into free space or water to meet diverse needs spanning communication, illumination, and display applications. Likewise, color converters can be integrated into receivers, where they convert incoming channel light to longer wavelengths, enabling superior coupling between optical signals and target PDs.

PQDs for indoor VLC transmitters

With the ongoing development of 6G technology, indoor VLC, as a crucial branch of OWC, has become a prominent research field. LiFi technology based on VLC systems is evolving and demonstrates the potential to significantly complement the indoor communication landscape currently dominated by WiFi[3,6,86-88]. Nevertheless, the VLC hardware infrastructure necessitates further refinement to achieve widespread commercial adoption. While VLC transmitters utilizing monochromatic light sources have reached a level of technological maturity, the integration of VLC transmitters with SSL sources, such as WLEDs and white laser diodes (WLDs), presents a more expansive opportunity[9,20]. The integration of color converter emissions with excitation sources constitutes a predominant strategy for generating high-quality white light. For PL white-light systems, excitation sources typically employ blue or UV band emission. Blue light is the most commonly used wavelength of pump source, as mature commercial WLEDs adopt the "partial conversion" principle, which combines blue GaN LED emissions with color-converting light components from phosphors[10]. As technological upgrades to traditional WLEDs, blue GaN μLEDs/LDs serve as ideal

excitation sources, demonstrating excellent luminous efficiency and modulation bandwidth (> GHz). Additionally, semiconductor light sources in the UV band are also utilized to excite color conversion materials[42]. Despite facing higher costs, lower external quantum efficiency, and reduced color conversion efficiency, the combination of UV LEDs/LDs with color converters still offers certain advantages for specific applications. For white lighting requiring high CRI, when white light is entirely emitted by color conversion materials, this approach facilitates achieving broader spectral coverage. Furthermore, this strategy enables dual-band communication across both UV and visible light spectra[89,90].

Recent years have witnessed significant advancements in VLC systems based on PL white-light sources[31,39,41]. WLEDs or WLDs with color converters typically exhibit reduced modulation bandwidths compared to monochromatic light sources. However, PQDs maintain relatively high bandwidths due to their shorter fluorescence lifetimes, with PQD-based WLED/WLD systems achieving the highest modulation bandwidths among research on PL white-light systems[26,31,41,53]. In 2018, Mei *et al.* developed a WLED-VLC system combining a blue GaN-based μLED with yellow-emitting $CsPbBr_{1.8}I_{1.2}$ QDs[39], demonstrating bandwidths of 73 MHz and 85 MHz for the PQDs and white-light system, respectively, with minimal degradation to 70 and 83 MHz after six months. The WLED achieved a maximum data rate of 300 Mbps. However, single yellow-emitting PQDs are insufficient to cover both the red and green spectral regions, which are critical for a high CRI, a metric essential for high-quality white lighting that requires values close to 100[19]. To achieve superior optical effects in white-light sources, the integration of at least two color converters with different peak wavelengths becomes imperative.

Color converters combining PQDs with other luminescent materials, including phosphors[29,30,45,51,60], II-VI semiconductor QDs[32,40,41], and organic emitters[53,54], have been reported. Although semiconductor QDs and organic emitters typically exhibit lower -3 dB bandwidths than PQDs, they all significantly surpass phosphors in terms of bandwidths. PQDs, when integrated as one of the color-converting components alongside more established luminescent materials, highlight their application potential in WLEDs. In 2021, Singh *et al.* demonstrated a flexible white-light system that utilized a semipolar blue InGaN/GaN μLED as the pump source, with $CsPbBr_3$ PQD paper and CdSe QD paper serving as green and red converters, respectively[41]. The semipolar μLED mitigated the QCSE, accelerating the radiative recombination process, and achieving a -3 dB bandwidth of 817 MHz and a data rate of 1.5 Gbps. The TRPL curves of the semipolar μLED, $CsPbBr_3$ PQD paper, and CdSe QD paper are illustrated in Figure 5A. The PQD paper exhibited a shorter average PL lifetime of 5.92 ns compared to 12.88 ns of the CdSe QD paper, attributable to the quantum confinement effect. Figure 5B compares the frequency responses and bandwidths between the PQD paper and a typical PQD film, with the PQD paper showing superior performance with a bandwidth of 229 MHz and a transmission rate of 400 Mbps. The white-light system and VLC test setup are depicted in Figure 5C. The -3 dB bandwidth of the WLED was limited to 95.5 MHz, due to a low bandwidth (< 25 MHz) of the red-emitting CdSe QD paper, underscoring the need to optimize the red component in this design. In 2022, Ali *et al.* developed a WLD by combining a blue LD with liquid-phase color converter (LCC) glass cavities containing green-emitting $CsPbBr_3$ and red-emitting CdSe/ZnS QDs[32]. The liquid-phase QDs exhibited enhanced thermal stability, which is attributed to free movement facilitating convective heat dissipation. Additionally, reduced self-aggregation in liquid-phase QDs contributed to improved optical performance and a faster radiative recombination process. This WLD achieved a CRI of 85 and a CCT of 5520 K, making it suitable for high-power, high-quality SSL. As shown in Figure 5D, under high-bandwidth blue LD excitation, the $CsPbBr_3$ QDs, CdSe/ZnS QDs, and WLD demonstrated -3 dB bandwidths of 883, 871, and 855 MHz respectively, with the WLD achieving a remarkable data rate of 2.1 Gbps.

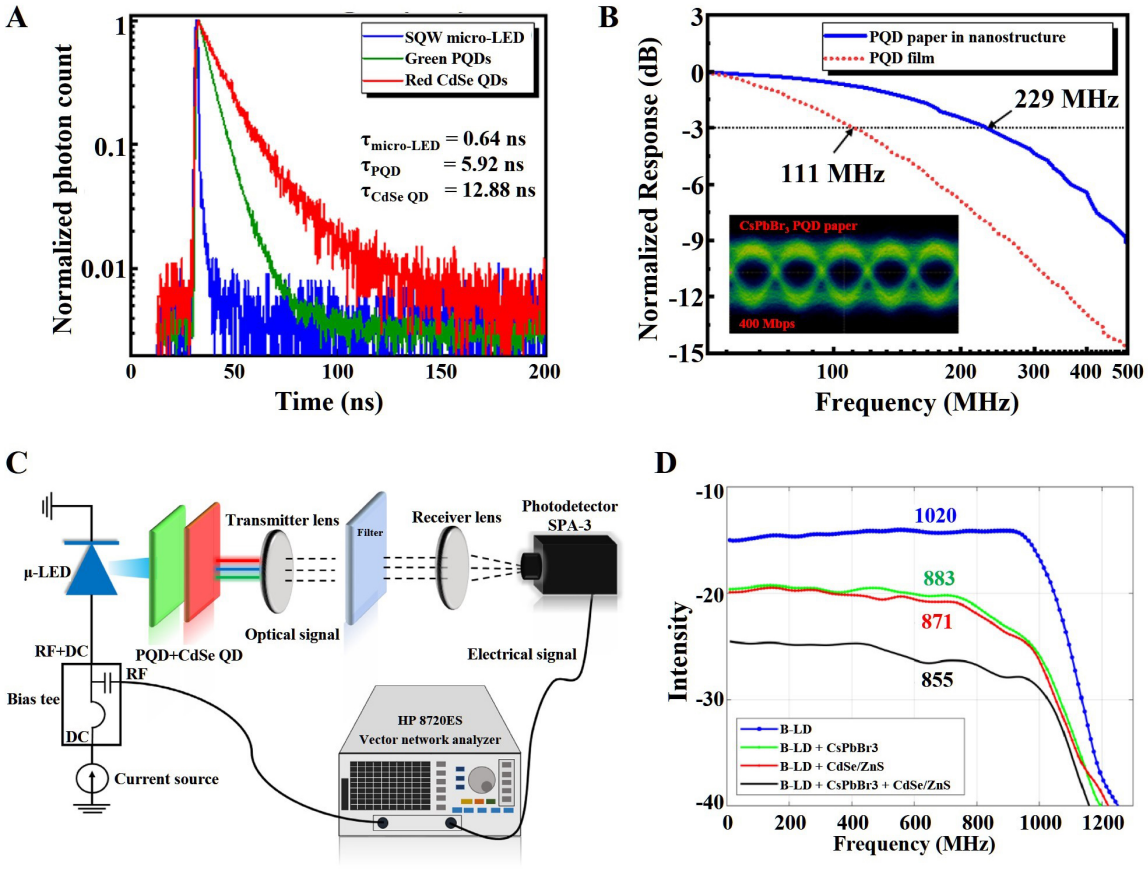

Figure 5. (A) TRPL curves for semipolar μLED, PQD paper, and CdSe QD paper; (B) frequency response and bandwidth of PQD paper and PQD film. Inset is an eye diagram for the PQD paper; (C) schematic of the white-light system setup for the VLC test; (D) frequency response of blue LD (B-LD) and B-LD with different QD converters. Reproduced with permission: (A-C)[41], Copyright 2021, Chinese Laser Press; (D)[32], Copyright 2022, Optica Publishing Group. SQW: single quantum well.

Considerable attention has been devoted to synthesizing perovskite/organic hybrid luminescent materials[53,54]. Organic emitters, compared to QDs, exhibit a broader spectrum, rendering them more suitable for high-CRI white-light illumination and complementing the spectral coverage limitations of PQD-based color converters. Studies have demonstrated that specific organic emitters can achieve high bandwidths exceeding 100 MHz[53,91-93], suggesting the potential for high-bandwidth performance in perovskite/organic hybrid materials. In 2024, Yao *et al.* fabricated a $CsPbBr_3$/organic color converter via an in situ solid-state synthesis technique[54]. The green-emitting $CsPbBr_3$ and red-emitting 2,3,5,6-tetrakis(3,6-diphenylcarbazol-9-yl)-1,4-dicyanobenzene (4CzTPN-Ph) formed multi-site contacts, establishing energy transfer channels that overcame the challenge of low light intensity from the red organic emitters. As illustrated by the energy transfer mechanism shown in Figure 6A, the green emission from $CsPbBr_3$ PQDs can indirectly excite 4CzTPN-Ph, thereby significantly enhancing the PL intensity of the organic red emission. When combined with a blue LED, the resulting WLED device achieved a CRI of 86 and a luminous efficacy (LE) of 100 lm/W. For VLC applications, the short PL lifetime (12 ns) of the color converter indicated the potential for high-speed transmission. The WLED demonstrated a data rate of 5 Mbps, limited by the substantial RC constant of the blue LED. Replacing the excitation source with a high-bandwidth alternative could further unlock the high-speed potential of this perovskite/organic hybrid color converter.

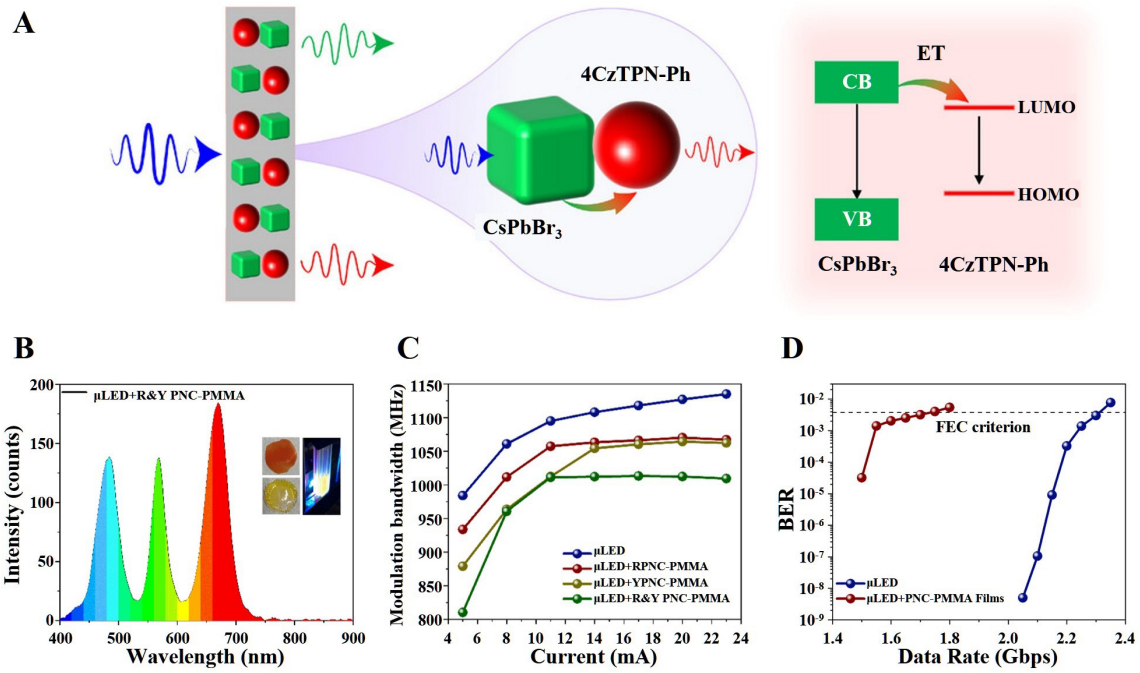

Figure 6. (A) Schematic of the enhanced organic red emission through energy transfer channels; (B) optical spectrum of the WLED. Insets are the photographs of red and yellow PNC-PMMA, and films cured in cuvettes; (C) modulation bandwidth of the system based on μLED and μLED with different PNC-PMMA films; (D) BER of μLED with and without PNC-PMMA films at different data rates. Reproduced with permission: (A)[54], Copyright 2024, Wiley-VCH GmbH; (B-D)[31], Copyright 2021, American Chemical Society. 4CzTPN-Ph: 2,3,5,6-tetrakis(3,6-diphenylcarbazol-9-yl)-1,4-dicyanobenzene; ET: energy transfer; CB: conduction band; VB: valence band; LUMO: lowest unoccupied molecular orbital; HOMO: highest occupied molecular orbital. PNC-PMMA: perovskite nanocrystal-polymethyl methacrylate; WLED: white light-emitting diode; μLED: micro light-emitting diode; BER: bit-error-rate.

In the aforementioned studies on hybrid luminescent materials, PQDs-based color converters typically exhibit shorter PL lifetimes and higher bandwidths. Consequently, developing color converters composed entirely of PQDs could further advance VLC applications. In 2021, Wang *et al.* employed yellow-emitting $CsPb(Br/I)_3$ and red-emitting $CsPbI_3$ PNC-PMMA films as color converters for blue μLEDs[31]. For SSL applications, the yellow/red-emitting PNC-PMMA films demonstrated FWHMs of 30 and 35 nm, respectively, which are sufficiently broad to support high-quality illumination. The WLED spectrum, depicted in Figure 6B, represents a warm white-light source with a CCT of 5670 K and a CRI of 75.7. In the VLC application, the yellow and red PNC-PMMA exhibited impressive modulation bandwidths of up to 347 and 822 MHz, respectively, owing to their exceptionally short PL lifetimes of 11.2 and 3.5 ns. Figure 6C illustrates the bandwidths of the μLED and three PNC-PMMA combinations under different driving currents. Attributed to the high bandwidths of PNC-PMMA, the modulation bandwidth at high currents only decreased from 1.130 GHz for the blue μLED to 1.005 GHz for the WLED. Figure 6D presents the BER of the μLED and WLED at different data rates under the NRZ-OOK modulation scheme. A record-breaking data rate of 1.7 Gbps was achieved for the white LED system while maintaining a BER below the FEC standard of 3.8×10^{-3}.

Physical multiplexing techniques, particularly WDM, can further exploit the data transmission potential of PQD-based VLC transmitters. In 2024, Fu *et al.* constructed a WDM-VLC system utilizing green/red-emitting liquid $CsPbBr_3/CsPbI_3$ QDs[46]. Benefiting from the wide-angle characteristics of liquid PQDs, the system achieved a field of view of ± 40° at a distance of 60 cm, with each green/red channel operating at 50 Mbps, yielding a total data rate of 100 Mbps. At the software level, the authors implemented a

computational temporal ghost imaging (CTGI) algorithm to reduce BER, extending the maximum transmission angle to ± 60°. The feasibility of WDM-VLC schemes utilizing PQD-based color converters with different emission wavelengths has been demonstrated. Further research should prioritize the enhancement of communication parameters of WDM-VLC systems, such as modulation bandwidth, data rate, transmission distance and angle. Table 2 summarizes the configurations and SSL-VLC parameters of recently developed PQD-based white-light systems. Future research should aim to advance WLED or WLD systems with variable CCT, higher CRI, increased transmission rates, and improved stability to enhance the practicality of SSL-VLC solutions.

PQDs for UWOC transmitters

With the advancement of underwater engineering such as marine exploration and environmental monitoring, there is an increasing demand for network connectivity among underwater devices. Consequently, UWOC has emerged as a significant research focus in recent years. UWOC, in conjunction with RF communication and underwater acoustic communication (UAC), is poised to meet the diverse requirements of the Internet of Underwater Things (IoUT) and underwater optical cellular networks. While UAC is distinguished by its capability in kilometer-range long-distance communication, UWOC has garnered attention for its advantages of low multipath loss, high transmission rate, low latency, and compact equipment size, rendering it highly suitable for last-meter solutions in underwater networking[94-97].

In pure water conditions, blue light undergoes minimal optical absorption loss, which is one of the reasons why blue LDs are extensively utilized in UWOC systems. Nevertheless, in actual aquatic environments, the wavelength that corresponds to the minimum loss shifts toward longer wavelengths as water turbidity increases[95,97,98]. PQDs are particularly advantageous as color conversion layers when paired with blue LDs to achieve green emission for UWOC applications, yielding two primary advantages. Firstly, while the "green gap" limits the electroluminescence efficiency of green diodes[98,99], the combination of blue LD and inorganic perovskite has demonstrated high efficiency in generating green light through a color conversion approach. Secondly, PQDs offer wavelength tunability, allowing for matching with the minimum-loss wavelength specific to different water environments. This flexibility enables UWOC systems to maintain minimal link loss[33,34].

As the first application of PQDs in UWOC, in 2021, Xia *et al.* integrated $CsPbBr_3$ NCs with a blue LD to construct a UWOC system operating over a 15 cm distance[33]. To enhance the stability of $CsPbBr_3$ NCs against water, heat, and intense laser irradiation of 3.6 kW/cm^2, they synthesized $CsPbBr_3$ NCs-glass through in situ precipitation in inorganic glass via solid-state reaction. This color converter achieved green emission with a narrow FWHM (~ 20 nm). Additionally, the high refractive index (1.54) of the glass matrix enhanced the radiative transition rates of $CsPbBr_3$ NCs, reducing the decay time to 3.22 ns. The experimental setup of the UWOC system is schematically depicted in Figure 7A. The study demonstrated a UWOC system with a bandwidth of 180 MHz and a data rate of 185 Mbps. As shown in Figure 7B, the eye diagram remained open after 60 minutes of operation, indicating the reliability of this UWOC system. Furthermore, Li *et al.* advanced PQD-based UWOC systems with improved transmission distance and networking capabilities. In 2022, the group developed a quasi-omnidirectional UWOC transmitter through the integration of liquid $CsPbBr_3$ QDs sealed in a cylindrical bottle with a blue LD, mitigating link alignment challenges[34]. Figure 7C and D presents the structure of this transmitter, and its uniform optical power distribution across the spherical surface. The UWOC system was validated in a standard swimming pool. Using on-off-keying (OOK) modulation, transmission rates of 60 Mbps and 40 Mbps were achieved at distances of 10 m and 20 m, respectively. With code division multiple access (CDMA) networking of four clients, each client reached 10 Mbps and 7.5 Mbps at 10 m and 20 m, respectively. Figure 7E demonstrates that in different communication modes, BER slightly increased with yaw angle changes, but the variations

Table 2. Parameters of PQD-based white-light systems for SSL-VLC applications

Year	Light source/Wavelength (nm)	Color converters/Wavelength (nm)	CRI	CCT	Bandwidth[a]	Data rate[b]	Refs.
2016	LD/450	$CsPbBr_3$/512	89	3236 K	1 GHz	2 Gbps	[29]
		Phosphor/ ~ 620					
2018	μLED/ ~ 445	$CsPbBr_{1.8}I_{1.2}$/ ~ 560	-	-	85 MHz	300 Mbps	[39]
2021	LED/ ~ 450	DDAB-$CsPbBr_3$/SiO_2/ ~ 515	88	3209 K	1.5 MHz	5.9 Mbps	[40]
		AgInZnS/ ~ 620					
2021	LED/450	$CsPbBr_3$@ZrO_2/ ~ 520	-	4743 K	2.75 MHz	33.5 Mbps	[51]
		$CaAlSiN_3$:Eu^{2+}/ ~ 620					
2021	μLED/ ~ 470	$CsPb(Br/I)_3$-PMMA/560	75.7	5670 K	1.005 GHz	1.7 Gbps	[31]
		$CsPbI_3$-PMMA/672					
2021	UV/280	$Cs_3Cu_2Cl_5$@SiO_x/523 $CaAlSiN_3$:Eu^{2+}/660	94	5049 K	420 kHz	2.65 Mbps	[60]
2022	LD/451	Liquid $CsPbBr_3$/511	85	5520 K	855 MHz	2.1 Gbps	[32]
		Liquid CdSe/ZnS/630					
2022	UV/300	$Cs_3Cu_2I_5$ SCs/444	91	5436 K	10.1 MHz	87.7 Mbps	[42]
		$CsCu_2I_3$ SCs/580					
2023	μLED/443	CC-MP3/477	82.4	5561 K	952 MHz	-	[53]
		$CH_3NH_3PbBr_3$/528					
		Ir(fbi)$_2$(acac)/568					
2023	UV/300	$Cs_3Cu_2Br_5$ SCs/464	81	6700 K	6.7 MHz	45 Mbps	[45]
		Phosphors/ ~ 550					
2024	LED/450	$CsPbBr_3$/530	86	4908 K	5 MHz	5 Mbps	[54]
		4CzTPN-Ph/580					

[a]modulation bandwidth of white-light system; [b]data rate of the white-light system. UV: ultraviolet light emitting diode; LED: light emitting diode; DDAB: didodecyldimethylammonium bromide; PMMA: polymethyl methacrylate; SC: single crystal; Ir(fbi)$_2$(acac): bis(2-(9,9-diethyl- fluoren-2-yl)-1-phenyl-1H-benzo[d] imidazolato)(actylacetonate)iridium(III); 4CzTPN-Ph: 2,3,5,6-tetrakis(3,6-diphenylcarbazol-9- yl)-1,4-dicyanobenzene; SSL: solid-state lighting; VLC: visible light communication; PQD: perovskite quantum dot; μLED: micro light-emitting diode; LD: laser diode; CCT: correlated color temperature; CRI: color rendering index.

remained within acceptable ranges. The authors noted that their design, incorporating a blue-emitting LD and a green-emitting $CsPbBr_3$ converter, could operate in dual modes: long-distance directional communication and short-distance omnidirectional communication, which could enhance the functionality of a single UWOC transmitter. The application of PQDs in UWOC transmitters has demonstrated initial promise for short-range underwater networking, and further research is needed to approach commercialization.

PQDs for photodetectors

In OWC systems, receivers play a pivotal role, and the link transmission rate is fundamentally constrained by the response characteristics of the receiver[1,9]. While color-converting PQDs are widely employed in transmitters, there is an emerging body of research that explores the placement of PQDs in proximity to PDs. This approach aims to convert the received light into specific wavelengths with a narrow FWHM to match the optimal spectral response of the target PDs. This strategy has the potential to significantly enhance the sensitivity and efficiency of PDs in OWC systems.

PQDs have been recognized for their potential in PDs for UV-based communication systems. UV light communication has emerged as a competitor to VLC due to its superior non-line-of-sight (NLOS) capability and reduced susceptibility to solar background radiation[89,90,100-102]. However, the development of efficient UV communication receivers presents several challenges. Traditional photomultiplier tubes

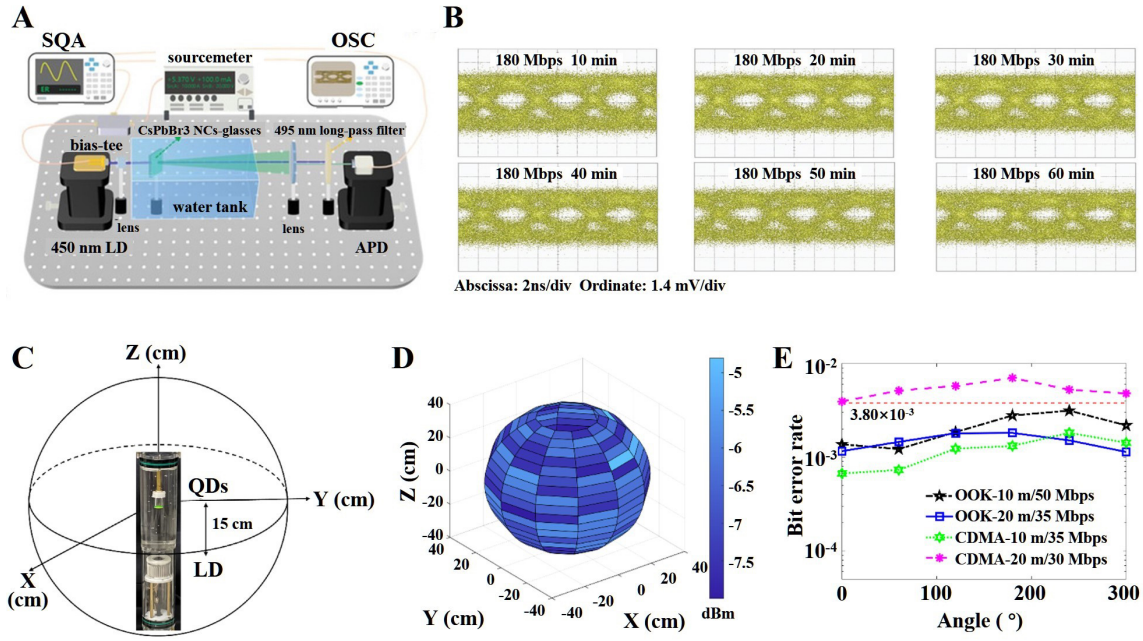

Figure 7. (A) Schematic of the experimental setup for the UWOC system based on $CsPbBr_3$ NCs-glass; (B) the eye diagrams for the UWOC system at different operating times; (C) structure of the quasi-omnidirectional UWOC transmitter; (D) measured optical power distribution of the UWOC transmitter; (E) BER for two communication modes at different yaw angles. Reproduced with permission: (A, B)[33], Copyright 2021, Wiley-VCH GmbH; (C-E)[34], Copyright 2022, Optica Publishing Group. SQA: signal quality analyzer; OSC: oscilloscope; APD: avalanche photodiode; UWOC: underwater wireless optical communication; NC: nanocrystal; BER: bit-error-rate.

(PMTs) are limited by high power consumption and large sizes[103], while III-nitride-based PDs face issues with dislocation and lattice mismatch[104]. Meanwhile, although Si-based PDs for visible light have reached technological maturity, they exhibit poor response to UV light[105]. Therefore, integrating PQD-based color converters with Si-based PDs offers an effective approach to UV detection. In 2019, Kang *et al.* developed a hybrid $CsPbBr_3$-silicon PD by integrating a $CsPbBr_3$ NCs layer with a Si-based PD[35]. $CsPbBr_3$ NCs can convert UVC (100-280 nm) light into green light, matching the high-response band of the Si-based PD. After installing the NCs layer in front of the bare Si-based PD, the responsivity to 270-nm UVC light increased from 29 to 84 mA/W. The PL decay time of $CsPbBr_3$ NCs was only 4.5 ns, enabling a small-signal modulation bandwidth of 70.92 MHz. Using a 278 nm UVC-LED as the transmitter with the OOK modulation scheme, the receiver achieved a data rate of 34 Mbps, compared to 25 Mbps without $CsPbBr_3$ NCs. In 2023, the same group incorporated $CsPbBr_3$ NCs in front of the optical concentrator of a Si-based receiver, expanding the FoV half-angle to 60°[36]. This improvement was attributed to $CsPbBr_3$ NCs acting as a secondary light source, emitting green light uniformly in 360°. Additionally, the data rates were improved to 100 Mbps and 71.6 Mbps under NRZ-OOK and OFDM modulation schemes, respectively. Figure 8A illustrates the experimental setup for UV light communication using the NRZ-OOK modulation scheme.

For the expansion of OWC receivers, perovskite fibers exhibit multifunctional characteristics. These fibers can facilitate wavelength conversion to better couple with PDs. Additionally, compared to planar-based PDs, perovskite fibers can form near-omnidirectional array reception platforms similar to radio-frequency antennas, owing to their inherent flexibility and scalability. This feature significantly reduces the difficulty of signal reception. In 2022, Kang *et al.* developed a near-omnidirectional OWC receiver based on perovskite-polymer-based scintillating fibers[44]. The design incorporated $CsPbBr_3$ NCs embedded within polymer fibers, which were cascaded and expanded to form a fiber PD array, coupled with either silica fibers or Si-

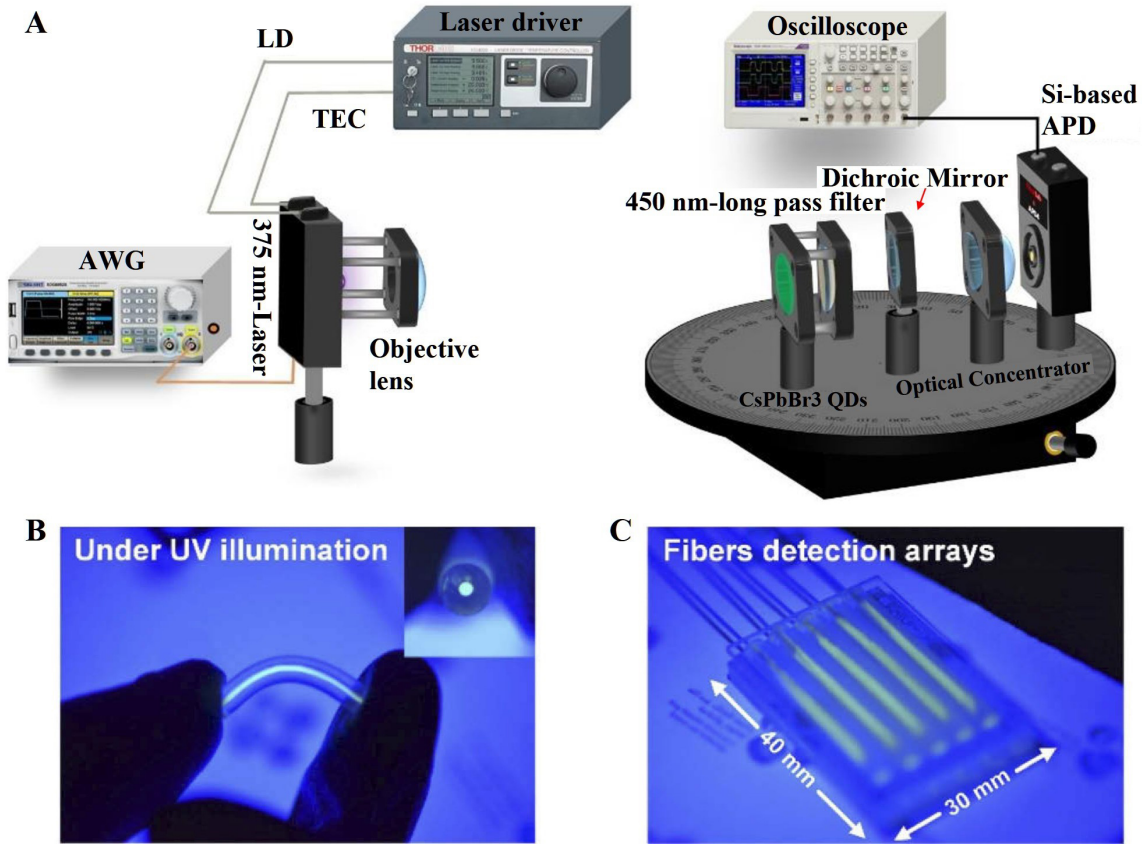

Figure 8. (A) Schematic of the experimental setup for UV light communication based on $CsPbBr_3$ NCs, using the NRZ-OOK modulation scheme; (B) image of the $CsPbBr_3$ NCs-polymer fiber under UV illumination; (C) image of the NCs-polymer fibers detection arrays. Reproduced with permission: (A)[36], Copyright 2023, Optica Publishing Group; (B, C)[44], Copyright 2022, Optica Publishing Group. AWG: arbitrary waveform generator; TEC: thermoelectric controller; APD: avalanche photodiode. NRZ-OOK: non-return-to-zero on-off keying; UV: ultraviolet; NC: nanocrystal.

based avalanche photodiodes (APDs). Figure 8B and C illustrates the $CsPbBr_3$ NCs-polymer fiber and its corresponding fiber detection arrays. Isobornyl acetate (IBOA) monomer was utilized to combine with $CsPbBr_3$ NCs to form a polymer composite. Although IBOA effectively enhanced the photostability of $CsPbBr_3$, it absorbed light at wavelengths below 400 nm, consequently limiting the communication band to the short-wavelength visible spectrum (400-475 nm). When transmitting data through the channel using 405 nm light, the perovskite-polymer-fibers re-emitted green light at approximately 514 nm. The system achieved data rates of 23 Mbps and 152.5 Mbps using NRZ-OOK modulation for VLC and OFDM modulation for UWOC, respectively. Both planar-based and fiber-based perovskite color-converting PDs have demonstrated their distinct advantages and application scenarios, offering promising strategies for advancing OWC receivers. Moreover, rapidly evolving perovskite PDs that directly perform photoelectric conversion are attracting increased attention. Compared to PQD-based color-converting PDs, photoelectric conversion perovskite PDs show promise as more versatile detection solutions due to their higher energy conversion efficiency and integration density[106-108].

CONCLUSIONS AND OUTLOOKS

OWC systems have emerged as a promising solution for next-generation 6G networks. For OWC systems employing color converters, PQDs have emerged as superior alternatives due to their exceptional optical properties and ultrafast response characteristics. To improve the modulation bandwidths and transmission

rates of PQD-based systems, this review first theoretically analyzes the critical factors, particularly emphasizing how size reduction and uniform dispersion of PQDs contribute to enhanced quantum confinement effect and carrier dynamics. Building on these foundations, researchers have implemented various strategies to improve the performance metrics and commercial viability of PQD-based SSL-OWC systems, encompassing developing high-bandwidth μLEDs or LDs as pump sources, optimizing PQD nanostructures and encapsulations, selecting appropriate modulation schemes and multiplexing techniques, and investigating the prospects of lead-free perovskites. Finally, the review comprehensively summarizes the evolution of PQD-based color converters across diverse OWC applications. Specifically, their implementation spans indoor VLC, UWOC, and UV light communication, where color-converting PQDs can be utilized in both transmitters and receivers.

Similar to perovskite color converters, electroluminescent perovskite light-emitting diodes (PeLEDs) are under development[109-111]. As light sources with tunable emission wavelengths, PeLEDs show promise for providing more integrated solutions for multi-wavelength systems, while avoiding energy losses caused by color conversion. However, currently, PeLEDs still lag significantly behind GaN light sources in terms of stability and modulation bandwidth (< 50 MHz). In contrast, color-converting OWC systems combining GaN μLEDs/LDs with PQDs have demonstrated performance advantages in WLED-VLC and UWOC applications, making this approach more feasible for commercialization.

Despite the unique optical and communication capabilities demonstrated by high-speed perovskite color converters, several critical challenges in PQD-based OWC systems warrant comprehensive investigation. Primarily, high-bandwidth semiconductor light sources, including μLEDs and LDs, encounter constraints regarding quantum efficiency, manufacturing yields, and thermal management. More significantly, research into fast-response PQD layers remains at a nascent stage of development. For both solid and liquid-phase PQD encapsulation approaches, there is an urgent need to develop optimization strategies that simultaneously achieve superior PLQY, high bandwidth, efficient thermal dissipation, and prolonged operational stability. Meanwhile, the development of lead-free perovskite materials for lighting and communications needs to be advanced. If the performance parameters of lead-free PQDs could match those of $CsPbX_3$ PQDs, they would provide high-bandwidth color converters with enhanced environmental compatibility. Additionally, real-time modulation and demodulation circuits must ensure latency minimization and system stability, while reducing heat generation and power consumption. As these technical challenges are progressively resolved, PQD-based SSL-OWC systems are positioned to become integral components of 6G infrastructure, establishing an extensive framework for the interconnected global communication system.

DECLARATIONS

Authors' contributions

Conceptualization and writing-original draft: Liu, R.; Yan, Z.; Wu, T.
Writing-review and editing, supervision, and funding acquisition: Wu, T.; Lu, T.; Chen, G.; Zheng, J.; Wang, S.; Y Lin, Y.; Su, Y.; Liao, X.; Lu, Y.; Kuo, H. C.; Chen, Z.

Availability of data and materials

Not applicable.

Financial support and sponsorship

This work was supported by the National Natural Science Foundation of China (62274138), the Natural Science Foundation of Fujian Province of China (2023J06012), Science and Technology Program of Fujian Province (Regional Development Program, 2024H4019), Fundamental Research Funds for the Central

Universities (20720230029), and Compound semiconductor technology Collaborative Innovation Platform project of FuXiaQuan National Independent Innovation Demonstration Zone (3502ZCQXT2022005).

Conflicts of interest

All authors declared that there are no conflicts of interest.

Ethical approval and consent to participate

Not applicable.

Consent for publication

Not applicable.

Copyright

REFERENCES

1. Chow, C. Recent advances and future perspectives in optical wireless communication, free space optical communication and sensing for 6G. *J. Lightwave. Technol.* **2024**, *42*, 3972-80. DOI
2. Khan, L.; Yaqoob, I.; Imran, M.; Han, Z.; Hong, C. 6G wireless systems: a vision, architectural elements, and future directions. *IEEE. Access.* **2020**, *8*, 147029-44. DOI
3. Haas, H.; Yin, L.; Chen, C.; et al. Introduction to indoor networking concepts and challenges in LiFi. *J. Opt. Commun. Netw.* **2020**, *12*, A190. DOI
4. Wei, Z.; Wang, Z.; Zhang, J.; Li, Q.; Zhang, J.; Fu, H. Evolution of optical wireless communication for B5G/6G. *Prog. Quantum. Electron.* **2022**, *83*, 100398. DOI
5. Chi, N.; Zhou, Y.; Wei, Y.; Hu, F. Visible light communication in 6G: advances, challenges, and prospects. *IEEE. Veh. Technol. Mag.* **2020**, *15*, 93-102. DOI
6. Haas, H.; Yin, L.; Wang, Y.; Chen, C. What is LiFi? *J. Lightwave. Technol.* **2016**, *34*, 1533-44. DOI
7. Yu, T.; Huang, W.; Lee, W.; Chow, C.; Chang, S.; Kuo, H. Visible light communication system technology review: devices, architectures, and applications. *Crystals* **2021**, *11*, 1098. DOI
8. James, S.; Huang, Y.; Ahmed, T.; et al. Micro-LED as a promising candidate for high-speed visible light communication. *Appl. Sci.* **2020**, *10*, 7384. DOI
9. Lu, T.; Lin, X.; Guo, W.; et al. High-speed visible light communication based on micro-LED: a technology with wide applications in next generation communication Opto Electron Sci 2022. p. 220020. DOI
10. Cho, J.; Park, J. H.; Kim, J. K.; Schubert, E. White light-emitting diodes: History, progress, and future. *Laser. Photonics. Rev.* **2017**, *11*, 1600147. DOI
11. Xiang, H.; Wang, R.; Chen, J.; Li, F.; Zeng, H. Research progress of full electroluminescent white light-emitting diodes based on a single emissive layer. *Light. Sci. Appl.* **2021**, *10*, 206. DOI PubMed PMC
12. Yan, Z.; Liu, S.; Sun, Y.; et al. Atomic layer deposition technology for the development of high-quality, full-colour micro-LED displays. *Next. Nanotechnology.* **2024**, *5*, 100051. DOI
13. Karpov, S. Carrier localization in InGaN by composition fluctuations: implication to the "green gap". *Photon. Res.* **2017**, *5*, A7. DOI
14. Anwar, A.; Sajjad, M.; Johar, M.; Hernández-gutiérrez, C.; Usman, M.; Łepkowski, S. Recent progress in micro-LED-based display technologies. *Laser. Photonics. Rev.* **2022**, *16*, 2100427. DOI
15. Zhou, X.; Tian, P.; Sher, C.; et al. Growth, transfer printing and colour conversion techniques towards full-colour micro-LED display. *Prog. Quantum. Electron.* **2020**, *71*, 100263. DOI
16. Cho, J.; Schubert, E. F.; Kim, J. K. Efficiency droop in light-emitting diodes: challenges and countermeasures. *Laser. Photonics. Rev.* **2013**, *7*, 408-21. DOI
17. Yang, X.; Lin, Y.; Wu, T.; et al. An overview on the principle of inkjet printing technique and its application in micro-display for augmented/virtual realities Opto Electron Adv 2022. p. 210123. DOI
18. Xu, Y.; Chen, J.; Zhang, H.; et al. White-light-emitting flexible display devices based on double network hydrogels crosslinked by YAG: Ce phosphors. *J. Mater. Chem. C.* **2020**, *8*, 247-52. DOI
19. Manousiadis, P. P.; Yoshida, K.; Turnbull, G. A.; Samuel, I. D. W. Organic semiconductors for visible light communications. *Philos. Trans. A. Math. Phys. Eng. Sci.* **2020**, *378*, 20190186. DOI PubMed PMC
20. Zhao, S.; Mo, Q.; Wang, B.; Cai, W.; Li, R.; Zang, Z. Inorganic halide perovskites for lighting and visible light communication. *Photon. Res.* **2022**, *10*, 1039. DOI
21. Huang, C. Y.; Li, H.; Wu, Y.; et al. Inorganic halide perovskite quantum dots: a versatile nanomaterial platform for electronic

applications. *Nanomicro. Lett.* **2022**, *15*, 16. DOI PubMed PMC

22. Chaudhary, B.; Kshetri, Y. K.; Kim, H. S.; Lee, S. W.; Kim, T. H. Current status on synthesis, properties and applications of $CsPbX_3$ (X = Cl, Br, I) perovskite quantum dots/nanocrystals. *Nanotechnology* **2021**, *32*, 502007. DOI
23. Protesescu, L.; Yakunin, S.; Bodnarchuk, M.; et al. Nanocrystals of cesium lead halide perovskites ($CsPbX_3$, X = Cl, Br, and I): novel optoelectronic materials showing bright emission with wide color gamut. *Nano. Lett.* **2015**, *15*, 3692-6. DOI PubMed PMC
24. He, X.; Li, T.; Liang, Z.; et al. Enhanced cyan photoluminescence and stability of $CsPbBr_3$ quantum dots via surface engineering for white light-emitting diodes. *Adv. Opt. Mater.* **2024**, *12*, 2302726. DOI
25. Pathak, S.; Sakai, N.; Wisnivesky, R. R. F.; et al. Perovskite crystals for tunable white light emission. *Chem. Mater.* **2015**, *27*, 8066-75. DOI
26. Ma, Z.; Li, X.; Zhang, C.; et al. $CsPb(Br/I)_3$ perovskite nanocrystals for hybrid gan-based high-bandwidth white light-emitting diodes. *ACS. Appl. Nano. Mater.* **2021**, *4*, 8383-9. DOI
27. Song, J.; Li, J.; Li, X.; Xu, L.; Dong, Y.; Zeng, H. Quantum dot light-emitting diodes based on inorganic perovskite cesium lead halides ($CsPbX_3$). *Adv. Mater.* **2015**, *27*, 7162-7. DOI
28. Xu, X.; Zhou, J.; Shi, Z.; et al. Microwave-assisted in-situ synthesis of low-dimensional perovskites within metal-organic frameworks for optoelectronic applications. *Appl. Mater. Today.* **2024**, *40*, 102418. DOI
29. Dursun, I.; Shen, C.; Parida, M. R.; et al. Perovskite nanocrystals as a color converter for visible light communication. *ACS. Photonics.* **2016**, *3*, 1150-6. DOI
30. Ali, A.; Tehseen, R.; Mithilesh, K.; et al. Blue-laser-diode-based high CRI lighting and high-speed visible light communication using narrowband green-/red-emitting composite phosphor film. *Appl. Opt.* **2020**, *59*, 5197-204. DOI
31. Wang, Z.; Wei, Z.; Cai, Y.; et al. Encapsulation-enabled perovskite-PMMA films combining a micro-LED for high-speed white-light communication. *ACS. Appl. Mater. Interfaces.* **2021**, *13*, 54143-51. DOI
32. Ali, A.; Qasem, Z.; Li, Y.; Li, Q.; Fu, H. All-inorganic liquid phase quantum dots and blue laser diode-based white-light source for simultaneous high-speed visible light communication and high-efficiency solid-state lighting. *Opt. Express.* **2022**, *30*, 35112-24. DOI
33. Xia, M.; Zhu, S.; Luo, J.; et al. Ultrastable perovskite nanocrystals in all-inorganic transparent matrix for high-speed underwater wireless optical communication. *Adv. Opt. Mater.* **2021**, *9*, 2002239. DOI
34. Li, X.; Tong, Z.; Lyu, W.; et al. Underwater quasi-omnidirectional wireless optical communication based on perovskite quantum dots. *Opt. Express.* **2022**, *30*, 1709-22. DOI
35. Kang, C.; Dursun, I.; Liu, G.; et al. High-speed colour-converting photodetector with all-inorganic $CsPbBr_3$ perovskite nanocrystals for ultraviolet light communication. *Light. Sci. Appl.* **2019**, *8*, 94. DOI PubMed PMC
36. Alshaibani, S.; Alkhazragi, O.; Ashry, I.; et al. Wide-field-of-view optical detectors for deep ultraviolet light communication using all-inorganic $CsPbBr_3$ perovskite nanocrystals. *Opt. Express.* **2023**, *31*, 25385-97. DOI
37. Leitão, M.; Islim, M.; Yin, L.; et al. Pump-power-dependence of a $CsPbBr_3$-in-Cs_4PbBr_6 quantum dot color converter. *Opt. Mater. Express.* **2019**, *9*, 3504. DOI
38. Shan, X.; Zhu, S.; Lin, R.; et al. Improvements of the modulation bandwidth and data rate of green-emitting $CsPbBr_3$ perovskite quantum dots for Gbps visible light communication. *Opt. Express.* **2023**, *31*, 2195-207. DOI
39. Mei, S.; Liu, X.; Zhang, W.; et al. High-bandwidth white-light system combining a micro-LED with perovskite quantum dots for visible light communication. *ACS. Appl. Mater. Interfaces.* **2018**, *10*, 5641-8. DOI
40. Li, X.; Cai, W.; Guan, H.; et al. Highly stable $CsPbBr_3$ quantum dots by silica-coating and ligand modification for white light-emitting diodes and visible light communication. *Chem. Eng. J.* **2021**, *419*, 129551. DOI
41. Singh, K.; Fan, X.; Sadhu, A.; et al. $CsPbBr_3$ perovskite quantum-dot paper exhibiting a highest 3 dB bandwidth and realizing a flexible white-light system for visible-light communication. *Photon. Res.* **2021**, *9*, 2341. DOI
42. Wang, B.; Chen, C.; Yang, X.; et al. Pressure-assisted cooling to grow ultra-stable $Cs_3Cu_2I_5$ and $CsCu_2I_3$ single crystals for solid-state lighting and visible light communication. *EcoMat* **2022**, *4*, e12184. DOI
43. Wu, T.; Lin, Y.; Huang, Y.; et al. Highly stable full-color display device with VLC application potential using semipolar μLEDs and all-inorganic encapsulated perovskite nanocrystal. *Photon. Res.* **2021**, *9*, 2132. DOI
44. Kang, C.; Alkhazragi, O.; Sinatra, L.; et al. All-inorganic halide-perovskite polymer-fiber-photodetector for high-speed optical wireless communication. *Opt. Express.* **2022**, *30*, 9823-40. DOI
45. Liang, D.; Tan, L.; Lu, S.; et al. Low-temperature solution synthesis of stable $Cs_3Cu_2Br_5$ single crystals for visible light communications. *ACS. Appl. Mater. Interfaces.* **2023**, *15*, 24622-8. DOI
46. Fu, Y.; Zhang, L.; Wangzhou, Y.; et al. Wavelength division multiplexing visible light communication with wide incident angle enabled by perovskite quantum dots. *Optics. Communications.* **2024**, *559*, 130427. DOI
47. Xu, X.; Fu, Y.; Shi, Z.; et al. Stable and self-healing perovskite for high-speed underwater optical wireless communication. *J. Mater. Chem. C.* **2024**, *12*, 3907-14. DOI
48. Qin, F.; Cao, Y.; Wang, C.; et al. $MAPbBr_3$@PbBr(OH) color converter for white light emission and underwater data transmission. *ACS. Appl. Opt. Mater.* **2025**, *3*, 169-77. DOI
49. Yang, J.; Wang, J.; Yin, Y.; Yao, H. Mitigating halide ion migration by resurfacing lead halide perovskite nanocrystals for stable light-emitting diodes. *Chem. Soc. Rev.* **2023**, *52*, 5516-40. DOI PubMed
50. Di, J.; Chang, J.; Liu, S. Recent progress of two-dimensional lead halide perovskite single crystals: crystal growth, physical properties, and device applications. *EcoMat* **2020**, *2*, e12036. DOI

51. Mo, Q.; Chen, C.; Cai, W.; Zhao, S.; Yan, D.; Zang, Z. Room temperature synthesis of stable zirconia-coated $CsPbBr_3$ nanocrystals for white light-emitting diodes and visible light communication. *Laser. Photonics. Rev.* **2021**, *15*, 2100278. DOI
52. Chang, Y.; Yoon, Y.; Li, G.; et al. All-inorganic perovskite nanocrystals with a stellar set of stabilities and their use in white light-emitting diodes. *ACS. Appl. Mater. Interfaces.* **2018**, *10*, 37267-76. DOI
53. Sadhu, A.; Pai, Y.; Chen, L.; Hsieh, C.; Lin, H.; Kuo, H. High bandwidth semipolar (20-21) micro-LED-based white light-emitting diodes utilizing perovskite quantum dots and organic emitters in color-conversion layers for visible light communication and solid-state lighting applications. *Nanoscale* **2023**, *15*, 7715-21. DOI PubMed
54. Yao, T.; Yang, Z.; Gu, L.; et al. In situ fabrication of multi-site contacted perovskite/organic hybrid color converter for indoor lighting and light communication. *Laser. Photonics. Rev.* **2025**, *19*, 2400758. DOI
55. Chang, Y.; Huang, Y.; Gunawan, W. H.; et al. 4.343-Gbit/s green semipolar (20-21) μ-LED for high speed visible light communication. *IEEE. Photonics. J.* **2021**, *13*, 1-4. DOI
56. Xu, F.; Jin, Z.; Tao, T.; et al. C-plane blue micro-LED With 1.53 GHz bandwidth for high-speed visible light communication. *IEEE. Electron. Device. Lett.* **2022**, *43*, 910-3. DOI
57. Rashidi, A.; Monavarian, M.; Aragon, A.; Rishinaramangalam, A.; Feezell, D. Nonpolar *m*-plane InGaN/GaN micro-scale light-emitting diode with 1.5 GHz modulation bandwidth. *IEEE. Electron. Device. Lett.* **2018**, *39*, 520-3. DOI
58. Li, Z.; Yu, L.; Liu, B.; et al. High-speed micro-LEDs based on nano-engineered InGaN active region towards chip-to-chip interconnections. *J. Lightwave. Technol.* **2024**, *42*, 8760-70. DOI
59. Li, Z.; Zhang, X.; Hao, Z.; et al. Bandwidth analysis of high-speed InGaN micro-LEDs by an equivalent circuit model. *IEEE. Electron. Device. Lett.* **2023**, *44*, 785-8. DOI
60. Zhao, S.; Chen, C.; Cai, W.; et al. Efficiently luminescent and stable lead-free $Cs_3Cu_2Cl_5$@silica nanocrystals for white light-emitting diodes and communication. *Advanced. Optical. Materials.* **2021**, *9*, 2100307. DOI
61. Luo, X.; Lai, R.; Li, Y.; et al. Triplet energy transfer from $CsPbBr_3$ nanocrystals enabled by quantum confinement. *J. Am. Chem. Soc.* **2019**, *141*, 4186-90. DOI
62. Qian, H.; Xiao, Y.; Liu, Z. Giant Kerr response of ultrathin gold films from quantum size effect. *Nat. Commun.* **2016**, *7*, 13153. DOI PubMed PMC
63. Ding, P.; Ko, P.; Geng, P.; et al. Strongly confined and spectrally tunable $CsPbBr_3$ quantum dots for deep blue QD-LEDs. *Adv. Opt. Mater.* **2024**, *12*, 2302477. DOI
64. Boehme, S.; Bodnarchuk, M.; Burian, M.; et al. Strongly confined $CsPbBr_3$ quantum dots as quantum emitters and building blocks for rhombic superlattices. *ACS. Nano.* **2023**, *17*, 2089-100. DOI PubMed PMC
65. Wei, Y.; Cheng, Z.; Lin, J. An overview on enhancing the stability of lead halide perovskite quantum dots and their applications in phosphor-converted LEDs. *Chem. Soc. Rev.* **2019**, *48*, 310-50. DOI
66. Triana, M.; Hsiang, E.; Zhang, C.; Dong, Y.; Wu, S. Luminescent nanomaterials for energy-efficient display and healthcare. *ACS. Energy. Lett.* **2022**, *7*, 1001-20. DOI
67. Li, S.; Pan, Y.; Wang, W.; Li, Y. $CsPbX_3$ (X = Cl, Br, I) perovskite quantum dots embedded in glasses: recent advances and perspectives. *Chem. Eng. J.* **2022**, *434*, 134593. DOI
68. Chen, S.; Lin, J.; Zheng, S.; Zheng, Y.; Chen, D. Efficient and stable perovskite white light-emitting diodes for backlit display. *Adv. Funct. Mater.* **2023**, *33*, 2213442. DOI
69. Sun, K.; Tan, D.; Fang, X.; et al. Three-dimensional direct lithography of stable perovskite nanocrystals in glass. *Science* **2022**, *375*, 307-10. DOI
70. Lin, X.; Han, Y.; Zhu, J.; Wu, K. Room-temperature coherent optical manipulation of hole spins in solution-grown perovskite quantum dots. *Nat. Nanotechnol.* **2023**, *18*, 124-30. DOI
71. Wang, Z.; Hou, L.; Li, J.; et al. Synthesis and optical wireless communication application of high efficiency extreme blue $CsPbBr_3$ nanoplates. *J. Mater. Chem. C.* **2024**, *12*, 5370-6. DOI
72. Yan, Z.; Liu, Z.; Yang, X.; et al. Perovskite quantum dot color conversion micro-LEDs: progress in stability and patterning. *Opto-Electron. Eng.* **2024**, *7*, 240088. DOI
73. Zhang, C.; He, Z.; Chen, H.; et al. Light diffusing, down-converting perovskite-on-polymer microspheres. *J. Mater. Chem. C.* **2019**, *7*, 6527-33. DOI
74. Zhu, S.; Qiu, P.; Shan, X.; et al. High-speed long-distance visible light communication based on multicolor series connection micro-LEDs and wavelength division multiplexing. *Photon. Res.* **2022**, *10*, 1892. DOI
75. Park, J.; Lee, E.; Park, S.; Raymond, S.; Pyo, S.; Jo, H. Modeling and analysis on radio interference of ofdm waveforms for coexistence study. *IEEE. Access.* **2019**, *7*, 35132-47. DOI
76. Yoshida, K.; Chen, C.; Haas, H.; Turnbull, G.; Samuel, I. RGB-single-chip OLEDs for high-speed visible-light communication by wavelength-division multiplexing. *Adv. Sci. (Weinh).* **2024**, *11*, e2404576. DOI PubMed PMC
77. Kim, D.; Park, H.; Jung, S.; et al. Visible-Light communication with lighting: RGB wavelength division multiplexing OLEDs/OPDs platform. *Adv. Mater.* **2024**, *36*, e2309416. DOI
78. Lu, T.; Dai, Y.; Lee, T.; et al. Experimental investigation of high-speed WDM-visible light communication using blue, green, and red InGaN μLEDs. *Opt. Lett.* **2024**, *49*, 4697-700. DOI
79. Wang, Z.; Jin, Z.; Lin, R.; et al. Vertical stack integration of blue and yellow InGaN micro-LED arrays for display and wavelength division multiplexing visible light communication applications. *Opt. Express.* **2022**, *30*, 44260-9. DOI

80. Hu, L.; Choi, J.; Hwangbo, S.; et al. Flexible micro-LED display and its application in Gbps multi-channel visible light communication. *NPJ. Flex. Electron.* **2022**, *6*, 234. DOI
81. Zhang, F.; Ma, Z.; Shi, Z.; et al. Recent advances and opportunities of lead-free perovskite nanocrystal for optoelectronic application. *Energy. Mater. Adv.* **2021**, *2021*, 2021/5198145. DOI
82. Fan, Q.; Biesold-McGee, G.; Ma, J.; et al. Lead-free halide perovskite nanocrystals: crystal structures, synthesis, stabilities, and optical properties. *Angew. Chem. Int. Ed. Engl.* **2020**, *59*, 1030-46. DOI
83. Ma, Z.; Ji, X.; Lin, S.; et al. Recent advances and opportunities of eco-friendly ternary copper halides: a new superstar in optoelectronic applications. *Adv. Mater.* **2023**, *35*, e2300731. DOI
84. Li, Y.; Zhou, Z.; Tewari, N.; et al. Progress in copper metal halides for optoelectronic applications. *Mater. Chem. Front.* **2021**, *5*, 4796-820. DOI
85. Shi, Y.; Liang, D.; Mo, Q.; et al. Highly efficient copper-based halide single crystals with violet emission for visible light communication. *Chem. Commun. (Camb).* **2023**, *59*, 583-6. DOI
86. Ghaderi, M. R. LiFi and hybrid WiFi/LiFi indoor networking: from theory to practice. *Opt. Switching. Networking.* **2023**, *47*, 100699. DOI
87. Zeng, Z.; Dehghani, S. M.; Wang, Y.; Wu, X.; Haas, H. Realistic indoor hybrid WiFi and OFDMA-based LiFi networks. *IEEE. Trans. Commun.* **2020**, *68*, 2978-91. DOI
88. Badeel, R.; Subramaniam, S.; Hanapi, Z.; Muhammed, A. A review on LiFi network research: open issues, applications and future directions. *Appl. Sci.* **2021**, *11*, 11118. DOI
89. Xiao, H.; Zhang, K.; Xu, B.; Shen, H.; Wang, L.; Sun, C. High-brightness green CdSe/ZnS quantum dots stimulated by solar-blind deep-ultraviolet light in optical wireless communications. *Opt. Lett.* **2024**, *49*, 3596-9. DOI
90. Memon, M.; Yu, H.; Jia, H.; et al. Quantum dots integrated deep-ultraviolet micro-LED array toward solar-blind and visible light dual-band optical communication. *IEEE. Electron. Device. Lett.* **2023**, *44*, 472-5. DOI
91. Zhang, Y.; Jiang, M.; Han, T.; et al. Aggregation-induced emission luminogens as color converters for visible-light communication. *ACS. Appl. Mater. Interfaces.* **2018**, *10*, 34418-26. DOI
92. Yang, X.; Shi, M.; Yu, Y.; et al. Enhancing communication bandwidths of organic color converters using nanopatterned hyperbolic metamaterials. *J. Lightwave. Technol.* **2018**, *36*, 1862-7. DOI
93. Sajjad, M.; Manousiadis, P.; Chun, H.; et al. Novel fast color-converter for visible light communication using a blend of conjugated polymers. *ACS. Photonics.* **2015**, *2*, 194-9. DOI
94. Yang, X.; Tong, Z.; Dai, Y.; et al. 100 m full-duplex underwater wireless optical communication based on blue and green lasers and high sensitivity detectors. *Opt. Commun.* **2021**, *498*, 127261. DOI
95. Spagnolo G, Cozzella L, Leccese F. Underwater optical wireless communications: overview. *Sensors. (Basel).* **2020**, *20*, 2261. DOI PubMed PMC
96. Ali, M.; Jayakody, D.; Li, Y. Recent trends in underwater visible light communication (UVLC) systems. *IEEE. Access.* **2022**, *10*, 22169-225. DOI
97. Zhu, S.; Chen, X.; Liu, X.; Zhang, G.; Tian, P. Recent progress in and perspectives of underwater wireless optical communication. *Prog. Quantum. Electron.* **2020**, *73*, 100274. DOI
98. Shi, J.; Niu, W.; Li, Z.; et al. Optimal adaptive waveform design utilizing an end-to-end learning-based pre-equalization neural network in an UVLC system. *J. Lightwave. Technol.* **2023**, *41*, 1626-36. DOI
99. Chen, H.; Lin, T.; Huang, F.; Li, S.; Tang, X.; Xie, R. Laser-driven high-brightness green light for underwater wireless optical communication. *Adv. Opt. Mater.* **2022**, *10*, 2200836. DOI
100. Yang, Y.; Hou, Y.; Wu, F.; et al. High wall-plug efficiency algan deep ultraviolet micro-leds enabled by an etched reflective array design for high data transmission. *IEEE. Trans. Electron. Devices.* **2024**, *71*, 3069-76. DOI
101. Maclure, D.; Chen, C.; McKendry, J.; et al. Hundred-meter Gb/s deep ultraviolet wireless communications using AlGaN micro-LEDs. *Opt. Express.* **2022**, *30*, 46811-21. DOI
102. Li, D.; Liu, S.; Qian, Z.; et al. Deep-ultraviolet micro-LEDs exhibiting high output power and high modulation bandwidth simultaneously. *Adv. Mater.* **2022**, *34*, e2109765. DOI
103. Eisaman, M.; Fan, J.; Migdall, A.; Polyakov, S. Invited review article: single-photon sources and detectors. *Rev. Sci. Instrum.* **2011**, *82*, 071101. DOI PubMed
104. Liang, Y.; Towe, E. Progress in efficient doping of high aluminum-containing group III-nitrides. *Appl. Phys. Rev.* **2018**, *5*, 011107. DOI
105. Shi, L.; Nihtianov, S. Comparative study of silicon-based ultraviolet photodetectors. *IEEE. Sensors. J.* **2012**, *12*, 2453-9. DOI
106. Zhou, Y.; Fei, C.; Uddin, M.; Zhao, L.; Ni, Z.; Huang, J. Self-powered perovskite photon-counting detectors. *Nature* **2023**, *616*, 712-8. DOI PubMed PMC
107. Chen, F.; Li, C.; Shang, C.; et al. Ultrafast response of centimeter scale thin $CsPbBr_3$ single crystal film photodetector for optical communication. *Small* **2022**, *18*, e2203565. DOI
108. Pan, X.; Zhang, J.; Zhou, H.; et al. Single-layer ZnO hollow hemispheres enable high-performance self-powered perovskite photodetector for optical communication. *Nanomicro. Lett.* **2021**, *13*, 70. DOI PubMed PMC
109. Shen, C.; Fang, S.; Zhang, J.; et al. High performance and stable pure-blue quasi-2D perovskite light-emitting diodes by multifunctional zwitterionic passivation engineering. *Adv. Photon.* **2024**, 6. DOI

110. Ren, A.; Wang, H.; Dai, L.; et al. High-bandwidth perovskite photonic sources on silicon. *Nat. Photon.* **2023**, *17*, 798-805. DOI
111. Bao, C.; Xu, W.; Yang, J.; et al. Bidirectional optical signal transmission between two identical devices using perovskite diodes. *Nat. Electron.* **2020**, *3*, 156-64. DOI PubMed PMC